A single cell atlas of the cycling murine ovary

Morris ME[1#*], Meinsohn MC[2,3*], Chauvin M[2,3+], Nguyen NMP[2,3+], Saatcioglu HD[2,3], Yuan S[2,3], Kashiwagi A.[2,3], Sicher NA. [2,3], Hyun M[4], Donahoe PK[2,3], Sabatini B[4], Pépin D[2,3#]

[1]Department of Gynecology and Reproductive Biology, Massachusetts General Hospital, Boston/MA, [2]Pediatric Surgical Research Laboratories, Massachusetts General Hospital, Boston/MA,[3]Department of Surgery, Harvard Medical School, Boston/MA, [4]Howard Hughes Medical Institute, Department of Neurobiology, Harvard Medical School, Boston/MA

Co-corresponding

*,+ Contributed equally

Abstract

The estrous cycle is regulated by rhythmic endocrine interactions of the nervous and reproductive systems, which coordinate the hormonal and ovulatory functions of the ovary. Folliculogenesis and follicle progression require the orchestrated response of a variety of cell types to allow the maturation of the follicle and its sequela, ovulation, corpus luteum (CL) formation, and ovulatory wound repair. Little is known about the cell state dynamics of the ovary during the estrous cycle, and the paracrine factors that help coordinate this process. Herein we used single-cell RNA sequencing to evaluate the transcriptome of > 34,000 cells of the adult mouse ovary and describe the transcriptional changes that occur across the normal estrous cycle and other reproductive states to build a comprehensive dynamic atlas of murine ovarian cell types and states.

Introduction

The ovary is composed of a variety of cell types which govern the dynamic functions of the ovary as both an endocrine organ capable of producing hormones such as sex steroids, and a reproductive organ

25 orchestrating follicular development, from a quiescent follicle until its ultimate ovulation. This process
26 necessitates precise coordination of germ cells and several different somatic cell types, including granulosa
27 cells, thecal cells, and stromal cells to support the growth of oocytes and their release, to produce the
28 necessary hormonal cues, as well as coordinate the profound tissue remodeling to accommodate these
29 dynamic developing structures. Furthermore, the state of each of these cells changes over the course of
30 the estrous cycle in a coordinated fashion to regulate waves of follicle growth and maturation, to time
31 ovulation precisely, and to provide hormonal support of potential pregnancy.
32
33 Single cell RNA sequencing has been used in a variety of tissues to obtain an in-depth understanding of
34 gene expression and cellular diversity. In the ovary, this technique has allowed us and others to explore
35 various physiologic processes during early ovarian development and ovarian aging (Zhao et al. 2020;
36 Stévant et al. 2019; Wagner et al. 2020; Niu and Spradling 2020; Jevitt et al. 2020; Man et al. 2020;
37 Meinsohn et al. 2021; Fan et al. 2019; Si Wang et al. 2020). For example, Fan et al. catalogued the
38 transcriptomic changes that occur during follicular development and regression and mapped the cell types
39 of the human ovary using surgical specimens (Fan et al. 2019). A primate model has been used to
40 investigate changes in cell types and states that occur in the ovary with aging (Si Wang et al. 2020) . Zhao
41 et al. looked at the development of the follicle during early embryonic ovarian development to discern the
42 relationship of oocytes to their support cells in formation of follicles (Zhao et al. 2020). We have used
43 scRNAseq to identify inhibitory pathways regulated by AMH during the first wave of follicular growth in the
44 murine ovary (Meinsohn et al. 2021). While all these studies have helped to establish a framework to
45 understand the major cell types in the ovary, it is important to describe the dynamic nature of cell states
46 across the estrous cycle at the single cell level.

47 To understand more fully the effect of cyclic endocrine, autocrine, and paracrine signals on ovarian cell
48 states we performed high-throughput single cell RNA sequencing of ovaries from adult mice across a
49 physiological spectrum of reproductive states. Ovaries were harvested from mice in the four phases of the
50 normal estrous cycle: proestrus, estrus, metestrus, and diestrus. Additionally, ovaries were evaluated from
51 mice that were lactating or non-lactating 10 days postpartum mice, and from randomly cycling adult mice.
52 Herein, we describe the somatic cell types of the ovary and their cycling states using single-cell

53 transcriptomics. Furthermore, we uncovered previously unrecognized complexity in the cellular subtypes
54 and their cyclic expression states which allowed us to identify secreted factors that vary across the estrous
55 cycle and therefore represent potential marker for staging.

56 **Methods**

57 **Mice**

58 Animal experiments were carried out in 6-8 weeks old C57BL/6 mice obtained from Charles River
59 Laboratory, approved by the National Institute of Health and Harvard Medical School Institutional Animal
60 Care and Use Committee, and performed in accordance with experimental protocols 2009N000033 and
61 2014N000275 approved by the Massachusetts General Hospital Institutional Animal Care and Use
62 Committee.

63 For the analysis of transcriptional changes in ovaries of cycling mice, animals were housed in standard
64 conditions (12/12 hours light/dark non-inverting cycle with food and water *ad libitum*) in groups of 5 with
65 added bedding from a cage that previously housed an adult male mouse to encourage cycling. Estrous
66 stage was determined by observation of the vaginal opening and by vaginal swabs done at the same time
67 daily, as previously described (Kano et al. 2017). Each mouse was monitored for a minimum of 2 weeks
68 to ensure its cyclicity. Four mice were sacrificed in each of the 4 phases of the estrous cycle and labeled
69 An additional 8 mice were included in the analysis and labeled
70 Four of these mice were lactating at day 10 postpartum and
71 four were 10 days postpartum with pups removed at delivery. Four additional mice were not monitored for
72 cycling and included to increase sample diversity.

73 Additional mice were monitored throughout the estrous cycle, to collect ovaries at each stage (groups of
74 N=5 for proestrus, estrus, metestrus, diestrus) for gene validation. Pairs of dissected ovaries were used to
75 extract mRNA for qPCR for one while the other was fixed in 4% paraformaldehyde for RNAish (RNAscope)
76 or immunohistochemistry to validate gene expression.

77 **Superovulation**

78 To stimulate superovulation, mature female mice (6-9 weeks C57BL/6) were injected IP with 5 IU of
79 pregnant mare serum gonadotropin (PMSG) (Calbiochem, San Diego, CA), followed 48 hours later by 5 IU
80 of human chorionic gonadotropin (hCG; Millipore Sigma, St. Louis, MO). The mice were euthanized 8 hours
81 after hCG treatment and ovaries harvested.

82 **Staging of estrous cycle by vaginal cytology**

83 As previously described (Byers et al. 2012; Kano et al. 2017), staging of mice was performed using a wet
84 cotton swab, introduced into the vaginal orifice then smeared onto a glass slide which was air-dried, stained
85 with Giemsa, and scored for cytology by two independent observers. Briefly, proestrus was determined if
86 the smear showed a preponderance of nucleated epithelial cells as well as leukocytes. Estrous was marked
87 by an abundance of cornified epithelial cells, while metestrous smears contained a mixture of cornified
88 epithelial cells and leukocytes. Finally, diestrus was characterized by abundant leukocytes with low
89 numbers of cornified epithelium or nucleated epithelial cells.

90 **Generation of single cell suspension**

91 Single cell suspension from mouse ovaries were obtained as previously described with uterine enzymatic
92 dissociation (Saatcioglu et al. 2019). Briefly, ovaries were incubated for 30min at 34C in dissociation
93 medium (82 mM Na_2SO_4, 30 mM K_2SO_4, 10 mM Glucose, 10 mM HEPES, and 5 mM $MgCL_2$, pH 7.4)
94 containing 15 mg of Protease XXIII (Worthington), 100 U Papain, with 5 mm L-Cysteine, 2.5 mM EDTA
95 (Worthington) and 1333 U of DNase 1 (Worthington). The reaction was then stopped in cold medium, and
96 samples were mechanically dissociated, filtrated, and spun down three times before being resuspended to
97 a concentration of 150,000 cells/mL in 20% Optiprep (Sigma) for inDrop sorting.

98 **Single-cell RNA sequencing (inDrops)**

99 Fluidic sorting was performed using the inDrop platform at the Single Cell Core facility at Harvard Medical
100 School as previously described (Klein et al., 2015, Macosko et al., 2015). We generated libraries of
101 approximately 1500 cells per animal which were sequenced using the NextSeq500 (Illumina) platform.
102 Transcripts were processed according to a previously published pipeline (Klein et al., 2015) used to build a

103 custom transcriptome from the Ensemble GRCm38 genome and GRCm38.84 annotation using Bowtie
104 1.1.1. Unique molecular identifiers (UMIs) were used to reference sequence reads back to individual
105 captured molecules, referred to as UMIFM counts. All steps of the pipeline were run using default
106 parameters unless explicitly specified.

107 **Single-cell RNAseq data analysis**

108 *Data processing*

109 The initial Seurat object was created using thresholds to identify putative cells (unique cell barcodes) with
110 the following parameters: 1000-20000 unique molecular identifiers, 500-5000 genes, and less than 15%
111 mitochondrial genes. The final merged dataset contained ~70000 cells which were clustered based on
112 expression of marker genes. These were further processed in several ways to exclude low-quality data
113 and potential doublets. Markers for each level of cluster were identified using MAST in Seurat.

114 *Volcano Plots*

115 Highly differentially expressed genes between different estrous cycles were identified using the function
116 FindMarkers in Seurat. Volcano plots were generated using ggplot2 package in R.

117 *Pathway Enrichment Analysis*

118 Differentially expressed genes with at least two-fold changes between contiguous estrous stages were used
119 as input for Gene Ontology Enrichment Analysis by clusterProfiler. Enrichplot package was used for
120 visualization. Biological process sub-ontology was chosen for this analysis.

121 *Pseudotime analysis*

122 Subsets of the granulosa cluster from preantral to corpus luteum (CL) stages and mesenchyme cluter were
123 extracted and a CellDataSet object was constructed by Monocle (version 2.14.0) (Trapnell et al. 2014). The
124 ordering genes were selected using differentially expressed markers between clusters, obtained by
125 following steps of reducing data

126

127

128 developmental stages. Heatmap representing the transcriptomic progression of dynamic genes in
129 the cell lineages of mesenchyme and granulosa clusters through the pseudotime was constructed
130 including early cells common to both lineages are located in the center (Prebranch) of the map,
131 with divergence to two different cell fates to the sides.

132 *Principal component analysis (PCA)*

133 PCA was used to identify common patterns of gene expression across stages of the cycle. For each
134 Level0 cluster object, cycling cells were extracted and genes that were expressed in more than 5% of
135 cells were identified. The expression of these genes in the cycling cells were scaled (set to mean zero,
136 standard deviation 1) and averaged across each of the 4 cycle stages. PCA was run (prcomp) on the
137 average scaled expression data.

138 **In situ hybridization and immunohistochemistry**

139 In situ hybridizations were done using kits from ACDBio as per and previously
140 described (Saatcioglu et al., 2019). Briefly, RNAish was performed with the RNAscope® 2.5 HD Reagent
141 Kit (RED, ACD Bio, # 322350; Duplex, ACD Bio, # 322500). Following deparaffinization in xylene,
142 dehydration, peroxidase blocking, and heat-induced epitope retrieval by the target retrieval and protease
143 plus reagents (ACD bio, #322330), tissue sections were hybridized with probes for the target genes (see
144 **Table S1** for accession number, target region, and catalog number of each gene) in the HybEZ hybridization
145 oven (ACD Bio) for 2 hours at 40°C. The slides were then processed for standard signal amplification steps,
146 and chromogen development. Slides were counterstained in 50% hematoxylin (Dako, #S2302), air dried,
147 and cover slipped with EcoMount. In addition to cycling and noncycling mice, superovulated mice were
148 used in some circumstances to specify transcripts from follicles associated with LH surge response and
149 from pre-ovulatory follicles at the estrous stage.

150 To combine RNAish staining with immunohistochemistry to identify smooth muscle actin protein, we first
151 processed the tissue section for RNAscope as described above, including deparafinazation, antigen

152 retrieval, hybridization and chromogen development. Sections were then blocked in 3% bovine serum
153 albumin (BSA) in Tris-buffered solution (TBS) for 1 hr. Following 3 washes with TBS, the sections were
154 incubated with a smooth muscle actin primary antibody (SMA) (1:300, Abcam) overnight at 4°C and
155 developed with Dako EnVision + System horseradish peroxidase (HRP). Labeled Polymer Anti-Rabbit was
156 used as the secondary antibody, and the HRP signal was detected using the DAKO detection system.
157 Slides were then counterstained in hematoxylin and mounted as described above.

158 **RT-qPCR**

159 Mice were monitored through the estrous cycle and sacrificed at specific stage/time-points as described
160 above. Ovaries were dissected and total RNA was extracted using the Qiagen RNA extraction kit (Qiagen,
161 # 74106). A cDNA library was synthesized from 500 ng total RNA using SuperScript III First-Strand
162 Synthesis System for RT-
163 051). The primers used for this study are described in **Table S2**. Expression levels were normalized to the
164

165 **ELISA**

166 Blood was collected from mice by facial vein puncture, incubated at RT until spontaneously clotted,
167 centrifuged at 8000rpm for 5min to collect the serum layer, and diluted 1/10 in each ELISA kit according to
168 the manufacturing protocol; Mouse CNP/NPPC ELISA kit (ref: NBP2-75790); Mouse serine protease
169 inactive 35 (PRSS35) ELISA kit (ref: MBS9717242); Mouse TINAGL1 / Lipocalin 7 ELISA kit (ref: LS-
170 F49684); and Human/Mouse/Rat Activin A Quantikine ELISA Kit (ref: DAC00B).

171 **Results:**

172 **scRNA-seq of adult mouse ovaries across reproductive states**

173 For single cell RNA sequencing we isolated the ovaries of 4 mice per group representing a range of
174 physiological reproductive states of sexually mature females including cycling (proestrus, estrus, metestrus,
175 diestrus), post-partum (day 10 post-partum non-lactating), lactating (day 10 postpartum lactating), and non-
176 monitored mice to increase sample diversity. Following enzymatic digestion of those ovaries, we generated
177 a single cell suspension and sorted by microfluidics with the inDROP methodology (Klein et al. 2015),

178 targeting 1500 cells per animal, and resulting libraries were indexed, combined, and sequenced together
179 (**Fig 1A**).

180 Following dimensionality reduction and clustering we identified multiple clusters which could be combined
181 to represent the major cell categories of the ovary (**Fig 1B**). To assign cell type identity we used cluster-
182 specific markers which were previously described in other studies or newly identified makers later validated
183 by RNA in situ (**Table S3**). The major clusters were composed of granulosa (N=17627 cells) and
184 mesenchymal cells composing the ovarian stroma (N=10825 cells). Many other minor cell types were
185 identified including endothelial cells (N= 3501 cells), ovarian surface epithelial cells (N=1088 cells), immune
186 cells (N=1649 cells), and oocytes (N=22 cells). The latter were poorly represented in the dataset possibly
187 due to cell size exclusion limitations of the technique, thus they are likely limited to small oocytes of
188 primordial follicles (**Fig 1B**). The heatmap of marker gene expression across the major categories of cell
189 types and states is represented in **Fig 1C**.

190 **Single cell sequencing reveals heterogeneity within granulosa and mesenchymal cell clusters**

191 *Mesenchyme*

192 The mesenchymal cluster is the second largest identified in our analysis after the granulosa cell cluster.
193 Based on prior studies (Fan et al. 2019; Si Wang et al. 2020a) we were able to further subcluster these
194 mesenchymal cells into three groups of theca: theca 1 (17%), theca 2 (16%), and thecal smooth muscle
195 cells (9%). Furthermore, we identified two stromal groups: stroma 1 (12%) and stroma 2 (31%), in addition
196 to pericytes (6%), and dividing mesenchyme (8%) as seen in **Fig 2A,** with the top 20 expressed markers of
197 each cluster described in **Table S4.**

198 Distinct transcriptional signatures were identified in the mesenchymal subclusters (**Fig 2B**), from which we
199 prioritized positive markers to validate based on highest fold-change expression, highest differential percent
200 expression, and lowest P-value **(Fig 2C)**.

201 Theca 1 cells could be defined by their expression of Small Cell Lung Carcinoma Cluster 4 Antigen (*Cd24a)*
202 and Hedgehog Interacting Protein (*Hhip);* meanwhile, theca 2 cells were identified by their expression of

203 Cytochrome P450 Family 17 Subfamily A Member 1 *(Cyp17a1)* suggesting they correspond to mature
204 steroidogenic theca. Theca externa was confirmed to express Microfibril Associated Protein 5 (*Mfap5)*
205 specifically by RNA in situ hybridization (**Fig 2C**). Furthermore, we observed co-localization of *Mfap5* and
206 Actin Alpha 2 (*Acta2,* also known as smooth muscle actin) in theca externa whereas *Hhip* was expressed
207 in theca interna and immature theca (**Fig S2A, B**). Stroma 1 and stroma 2 compartments were validated
208 by their expression of Ectonucleotide Pyrophosphatase/Phosphodiesterase 2 (*Enpp2)* and Potassium Two
209 Pore Domain Channel Subfamily K Member 2 (*Kcnk2)*, respectively, and overlapped in distribution in both
210 cortical and medullary regions of the ovarian stroma (**Fig 2C**).

211 *Granulosa*

212 To explore further the cellular heterogeneity of developing follicles, we investigated the granulosa cell
213 compartment. Consistent with previous reports, we could distinguish granulosa cells of follicles based on
214 their stage of development (Gallardo et al. 2007; Fan et al. 2019; Zhao et al. 2020). Granulosa cells could
215 be subdivided into 8 main categories: pre-antral/cumulus (27%), antral/mural (25%), periovulatory (5%),
216 atretic (17%), mitotic (16%), and three clusters of corpus luteum: CL1 (2%), CL2 (4%), and CL3 (4%) (**Fig**
217 **3A). Table S5** lists the top twenty markers for each of these clusters. Distinctive gene expression programs
218 were identified in the granulosa cell subclusters, as visualized in the heatmap (**Fig 3B**), from which we
219 selected potential markers for validation.

220 Early pre-antral granulosa cells, and those constituting the cumulus of antral follicles, could be defined by
221 their shared expression of markers such as potassium channel tetramerization domain (Kctd14) (**Fig 3C**).
222 In contrast, expression of *Male-specific Transcription in the developing Reproductive Organs* (MRO) was
223 found specifically in mural granulosa cells of antral follicles (**Fig 3C**). Periovulatory follicles could be
224 characterized by their specific expression of the RUNX1 family transcription factor 1 (*Runx1*) (**Fig 3C**).
225 Furthermore, we identified three different clusters that we speculate represent cells/states of the corpus
226 luteum, CL-1, CL-2, CL-3, which all expressed One Cut Homeobox 2 (*Onecut2).* Finally, two relatively
227 abundant granulosa cell states could be identified based on marker expression, namely mitotic granulosa
228 cells expressing topoisomerase 2a (*Top2a*), and putative atretic cells expressing markers consistent with
229 follicular atresia including expression of the growth hormone receptor (*Ghr*) **(Fig3 C)**.

230 **Pseudotime analysis reveals differentiation lineages in mesenchyme and granulosa cell subtypes**

231 To examine the relationship between subpopulations of granulosa and mesenchyme cells, we performed
232 pseudotime trajectory analysis using the Monocle algorithm (Trapnell et al. 2014). In the mesenchyme we
233 included the theca 1 & 2, stroma 1&2, and smooth muscle clusters **(Fig4 A, B, C),** but omitted the pericytes.
234 For granulosa cells we included preantral/cumulus, antral/mural, periovulatory, and corpus luteum clusters
235 CL1-3, (**Fig 4 D, E, F**), but omitted the mitotic and atretic clusters. In both cases, the analysis revealed 3
236 states and 1 branch point (**Fig 4**). In the me
237
238 both stroma 1&2 clusters. At the branch point, stromal cells were ordered in one branch while both theca
239 clusters and smooth muscle were ordered on other branches **(Fig 4 A, B)** suggesting these are distinct and
240 non-overlapping differentiation programs that may be activated in either stroma 1 or stroma 2 and
241 supporting the notion that theca 1 (immature) represents a precursor to theca 2 (steroidogenic) **(Fig 4C)**.
242 For the granulosa cell subclusters of preantral granulosa, and at the
243 branching point, there we two cell fates: either cumulus and antral/mural granulosa ordered on one branch
244 or the three different corpus luteum clusters (CL1-3) and the periovulatory cluster ordered on another
245 branch **(Fig 4 D ,E).** This branching pattern supports the notion that the cumulus state is a continuation of
246 the early preantral granulosa program, while the distinct branching fate of periovulatory and CL2 represents
247 a continuum of differentiation states corresponding to the LH-response in granulosa cells and induction of
248 the luteinizing program **(Fig 4F)**. Heatmaps were constructed to represent the transcriptomic progression
249 of dynamic genes in the cell lineage of mesenchyme **(Fig S4 A)** and granulosa cells **(Fig S4B)** clusters
250 through pseudotime.

251 **Granulosa cells transcriptome varies most between proestrous and estrous stages**

252 We then focused on the granulosa cell cluster to identify the cell states associated with the stage of the
253 estrous cycle. When comparing the composition of granulosa cell subclusters by estrous stage, we found
254 that some clusters were dominated by cells from either the proestrous and estrous ovaries, particularly the
255 (**Fig 5A**). A volcano plot
256 analysis confirmed that the transition between these two stages was characterized by 22 significantly

257 upregulated and 4 significantly downregulated markers (**Fig 5B**), which represent a bigger population of
258 differentially regulated genes than those found at any other stage transition i.e., estrus to metestrus,
259 metestrus to diestrus, and diestrus to proestrus (**Fig S5A, B, C**). Gene ontology analysis revealed that the
260 most significantly differentially regulated pathways between the proestrous and estrous states were ovarian
261 matrix remodeling related processes and steroidogenesis and hormones production (**Fig 5C**). Whole ovary
262 qPCR validated these significant changes in expression at the proestrus to estrus transition in markers
263 involved in steroidogenesis, such as, Cytochrome P450 Family 19 Subfamily A Member 1 *(Cyp19a1*,
264 p=0.0029, proestrus to estrus*)*, Steroidogenic Acute Regulatory Protein (*Star,* p=0.0187, proestrus to
265 estrus) or Prosaposin (*Psap*, p=0.0026, proestrus to estrus*),* as well as matrix remodeling processes such
266 as Regulator Of Cell Cycle (*Rgcc*, p=0.0441, proestrus to estrus), Glutamate-Ammonia Ligase *(Glul)* and
267 Inhibitor Of DNA Binding 2 *(Id2,* p=0.0032, proestrus to metestrus*)* (**Fig 5D**), and immediate early genes,
268 Fos Proto-Oncogene (*Fos*), Jun Proto-Oncogene (*Jun*, p=0.0022, proestrus to estrus), Jun Proto-
269 Oncogene B (*Junb*, p=0.0069, proestrus to diestrus) and Early Growth Response 1 (*Egr1*, p=0.0504 estrus
270 to diestrus), involved in wound repair following ovulation **(Fig S5D)**.

271 **Identification and validation of secreted biomarkers varying throughout the estrous cycle**

272 To identify new biomarkers varying as a function of the estrous cycle that could be used for staging in
273 assisted reproduction and other applications in reproductive medicine, we focused on secreted factors that
274 could be therefore readily detectable in the blood and expressed mostly in the granulosa cell or ovarian
275 mesenchyme clusters to provide tissue specificity. We confirmed our ability to detect gene expression
276 changes during the cycle using whole ovary qPCR analysis in a sperate set of staged mice (N=4 per group),
277 with the well-described markers, Luteinizing Hormone/Choriogonadotropin Receptor (*Lhcgr*, p=0.0281
278 etrus to metestrus) and progesterone receptor (*Pgr,* p=0.0096, proestrus to estrus) (**Fig 6A**). Most
279 prominently we identified within our scRNAseq dataset, natriuretic peptide C (*Nppc*) and Inhibin A *(Inhba),*
280 as secreted markers that were significantly upregulated in the proestrous stage compared to the estrous
281 stage in the scRNAseq dataset (**Fig 6B**), which we validated by qPCR (*Nppc*, p=0.0022 proestrus to estrus,
282 *Inhba*, p= 0.0067, proestrus to estrus) (**Fig 6A**). Similarly, Tubulointerstitial Nephritis Antigen Like 1
283 (*Tinagl1*) and Serine Protease 35 (*Prss35*) were secreted markers significantly upregulated in estrous

284 compared to their level of transcription in proestrus in the scRNAseq dataset (**Fig 6B**), and by qPCR
285 (*Tinagl1* p=0.0081 proestrus to estrus, *Prss35* p=0.0008 proestrus to estrus) (**Fig 6A**). In situ RNA
286 hybridization showed, as expected, that these markers were mostly expressed in mural granulosa cells of
287 antral follicles, while *Nppc* was expressed in both mural and cumulus cells (**Fig 6C**). Finally, we sought to
288 quantify the abundance of secreted PRSS35, NPPCC, TINAGL1 and ACTIVIN A proteins in the serum of
289 staged mice by ELISA (**Fig 6D**). We found that ACTIVIN A concentration in serum was significantly
290 increased between the diestrous and proestrous stages (p=0.0312) and peaked at the proestrous stage
291 (**Fig 6D**), similar to the *Inhba* transcript which encodes for the ACTIVIN A beta subunit (**Fig 6A**), although
292 unlike the mRNA the protein remained elevated during the estrous stage (**Fig 6D**). Circulating PRSS35
293 levels were lowest at the metestrous stage and were significantly increased during the transition to diestrus
294 (p=0.0009) and remained significantly elevated until the proestrus (**Fig 6D**), which contrasts with the Prss35
295 transcript which was significantly induced at estrus (**Fig 6A**). The serum concentrations of TINAGL1 which
296 was lowest at the diestrous and proestrous stages, was significantly increased during the transition between
297 proestrus and metestrus, peaking in estrus (p=0.0142) (**Fig 6D**), which coincided with the transcriptional
298 pattern observed by qPCR and scRNAseq (**Fig 6A, 6B**). We observed a trend for serum protein
299 concentrations of NPPC to be lowest at the proestrous and estrous stages and increase during the
300 metestrous and diestrous stages (**Fig 6D**), although the differences were not statistically significant
301 (p=0.0889, estrus to metestrus). Importantly, these four markers could help identify the four different stages
302 of the estrous cycle when measured in conjunction in the blood (**Fig 6E**).

303 **Discussion**

304 Single cell RNA sequencing has been used to catalog the transcriptomes of a variety of tissues in several
305 species, across different physiological states (Hwang, Lee, and Bang 2018). Herein, we used scRNAseq
306 to catalog the cellular diversity and the changing cell states of the mouse ovary across the estrous cycle
307 and other reproductive states. In particular, we described the diversity of cell types and cell states of the
308 ovarian granulosa and mesenchymal cell subtypes, identified marker genes and cycling states for these
309 cells, and evaluated secreted markers for assessment of cyclic stages which may have utility for assisted
310 reproduction.

311 Given our focus on estrous cycle states, and the importance of granulosa cells in cyclic follicle maturation
312 and hormone production, it is unsurprising that this cluster was the most variable in gene expression and
313 contained the highest subclustering complexity. Some of this subclustering reflected transcriptomic
314 changes associated with estrous cycling; indeed, while most of the granulosa subclusters contained similar
315 amounts of cells from the proestrus, metestrus, and diestrus samples, o -ovulatory
316
317 been previously reported to be involved in the ovulatory process and regulated by the LH surge, including
318 markers of terminal differentiation and steroidogenesis such as Smarca1 (Lazzaro et al. 2006), Cyp11a1
319 (H. F. Irving-Rodgers et al. 2009) and Mt1 and Mt2 (Shujuan Wang et al. 2018). Other genes enriched in
320 this subcluster such as Prss35 (Wahlberg et al. 2008) and Adamts1(Lussier et al. 2017; Sayasith, Lussier,
321 and Sirois 2013) had been previously identified as involved in follicular rupture which is a process necessary
322 for ovulation during estrus.

323 While the ovulatory antral follicle is unique to the estrous stage, most other follicle types can be found at all
324 estrous cycle stages, albeit in varying numbers. Early pre-antral follicles numbers are relatively stable
325 across the estrous cycle (Deb et al. 2013), given that they are largely unresponsive to gonadotropins (J. S.
326 Richards 1980), in contrast antral follicle numbers and size are more variable (Deb et al. 2013). Some
327 markers were unique to preantral follicles, as previously noted by others, including Col18a1 (Melo et al.
328 2017; Helen F. Irving-Rodgers et al. 2010; Diaz, Sugiura, and Eppig 2008) and Wnt4 (Hsieh et al. 2002).
329 The antral granulosa subcluster could be identified by its expression of Inha as previously described (Chen
330 et al. 2009; Wigglesworth et al. 2015). By comparing clustering of preantral and antral granulosa cells by
331 single cell transcriptomics to the expression of these markers by RNAscope, we found interesting parallels
332 between granulosa cells of preantral follicles and cumulus cells of antral follicles which shared many
333 markers that were absent from mural granulosa cells. These differences between preantral and antral
334 follicle mural granulosa cells were reflected in pseudotime trajectory analysis, suggesting that the preantral
335 granulosa cell states are conserved in the cumulus cells of antral follicles while the mural granulosa cells
336 of antral follicles are further differentiated and form a separate branch in the pseudotime trajectory. An
337 example of shared marker expression between preantral and cumulus granulosa is Kctd14, a member of
338 the Potassium Channel Tetramerisation Domain Containing family in granulosa cells expressed during the

339 initial growth of early pre-antral follicles, which we had previously shown to be regulated by AMH (Meinsohn
340 et al., 2021). RNAscope analysis of Kctd14 expression identified a group of cells present in preantral
341 follicles directly adjacent to the oocyte that were destined to differentiate into cumulus cells of large antral
342 follicles. To date the function of KCTD14 in the ovary remains unknown.

343 The cluster designated as corpus luteum could be divided into three subclusters (CL_1-3), which we
344 speculate might represent different life stages of the developing corpus luteum. Supporting this
345 interpretation, pseudotime analysis of granulosa cell trajectories found that the CL_2 cluster was closer to
346 the periovularory granulosa cells, suggesting it may be composed of early differentiating luteal cells
347 characterized by their transcriptional response to the LH surge. The gene expression signature of the CL_2
348 cluster confirms that these cells are involved in active steroid production, as evidenced by the high
349 expression of Star (Kiriakidou et al., 1996), and Hsd17b7, (Stocco et al., 2007). The CL_3 cluster was
350 comprised of luteal cells expressing markers such as the Nuclear Paraspeckle Assembly Transcript 1
351 (Neat1), which has been shown to be involved in the successful formation of the corpus luteum, as most of
352 the Neat1 KO mice fail to establish corpora lutea leading to successful pregnancies due to low levels of
353 progesterone (Nakagawa et al. 2014). The CL_1 cluster which the pseudotime profile places in proximity
354 to CL_3, appears to share features of both CL_2 and CL_3. Future studies will be needed to further define
355 these corpus luteum expression signatures and determine if they represent cell states corresponding to the
356 natural progression of the CL from formation to regression (periovulatory>CL_2>CL_1>CL_3) or distinct
357 luteal cell subtypes reflecting different cellular origins or distinct functions.

358 The final two granulosa subclusters can be identified as mitotic and atretic cells based on their expression
359 of previously validated markers. Indeed, transcripts enriched in the latter are consistent with markers of
360 atretic follicles including Caldesmon 1 (Cald1) (Hatzirodos et al. 2014), Phosphoinositide-3-Kinase
361 Interacting Protein 1(Pik3ip1) (Piersanti et al. 2019), Thrombospondin 1 (Thbs1) (Thomas et al. 2008;
362 Garside et al. 2010; Zhu et al. 2019), and SRY-Box Transcription Factor 4 (Sox4) (Terenina et al. 2017;
363 Fan et al. 2019). While markers found in mitotic granulosa cells are universally characteristic of dividing
364 cells (**Table S5**).

365 The mesenchymal cluster was also surprisingly complex and somewhat variable across the estrous cycle,
366 reflecting its physiological and temporal function to accommodate the dynamic tissue remodeling
367 associated with follicle growth, steroid hormone production, and ovulation. The ovarian stroma adjacent to
368 the developing follicle is thought to differentiate into the theca, which is responsible for steroid hormone
369 biosynthesis and therefore underlies the cyclic hormone production of the ovary (RYAN and PETRO 1966).
370 Here we identified two theca clusters, designated as Theca 1 and 2. Theca 1, defined by markers such as
371 Hhip (Hummitzsch et al. 2019; JoAnne S. Richards et al. 2018), Mesoderm Specific Transcript (Mest) (Fan
372 et al. 2019), and Patched 1 (Ptch1) (JoAnne S. Richards et al. 2018; Fan, et al. 2019), was presumed to
373 be immature theca. As the follicle matures and the antrum forms, this layer becomes vascularized and
374 differentiates into theca interna, which is steroidogenic. This steroidogenic theca cluster (Theca 2), was
375 readily identifiable through its expression of Hydroxy-Delta-5-Steroid Dehydrogenase, 3 Beta- and Steroid
376 Delta-Isomerase 1 (Hsd3b1), Cyp17a1, Cyp11a1 (Fan, et al. 2019), Fdx1 (Fan et al. 2019) and Prolactin
377 receptor (Prlr) (Grosdemouge et al. 2003). Theca externa, which plays a structural role in the follicle, is
378 comprised of smooth muscle cells, and was identified by its expression of structural proteins such as Myosin
379 Heavy Chain 11 (Myh11), Transgelin (Tagln), and Smooth Muscle Actin (Sma or Acta2) (Zhao et al. 2020).
380 Interestingly Fan et al. (2019) also identified a smooth muscle cluster remarkable for its high expression of
381 structural genes such as Collagen Type I Alpha 1 Chain (Col1a1), Collagen Type I Alpha 2 Chain (Col1a2),
382 Collagen Type 6 Alpha 1 Chain (Col6a1) and Collagen Type 6 Alpha 2 Chain (Col6a2) (Fan et al. 2019).
383 In our dataset these genes were expressed in the smooth muscle, theca 1, and both stromal 1&2 clusters
384 (Fan et al. 2019). Another difference was their report of Aldehyde Dehydrogenase 1 Family Member A1
385 (Aldh1a1) expression in theca externa which we found primarily in the cluster theca 2 in our dataset. These
386 differences could be attributable to clustering resolution and species variation.

387 The rest of the ovarian mesenchyme was subdivided into two stromal clusters, labelled stroma 1 and stroma
388 2. It is tempting to speculate that stroma 1 and 2 may represent two distinct populations of stromal cells
389 which differ in abundance according to their position in the cortex or medulla or their proximity to follicles,
390 but our RNAscope analysis could not conclusively distinguish any unique histology or spatial mapping. The
391 genes enriched in these clusters were consistent with previous work, including extracellular matrix and cell
392 adhesion (e.g. Decorin (Dcn), Lumican (Lum), Col1a1), transcriptional machinery (e.g. SRY-Box

393 Transcription Factor 4 (Sox4), GATA Binding Protein 6 (Gata6)), and TGFB signaling (e.g. Latent
394 Transforming Growth Factor Beta Binding Protein 4 (Ltbp4), HtrA Serine Peptidase 3 (Htra3)) markers
395 (Kinnear et al. 2020).

396 The ovarian surface epithelium (OSE) is a simple mesothelial cell layer covering the ovarian stroma which
397 is disrupted during ovulation and dynamically expands and contracts with cyclic ovarian changes (Hartanti
398 et al. 2019; Xu et al. 2011). The OSE was represented by fewer than 3% of all cells (845 cells) in our
399 dataset and could be identified based on well-established markers such as keratin (Krt) 7, 8 and 18
400 (Kenngott et al. 2014), Metallothioneins Mt1 (Iwata et al. 1999) and Mt2 (Iwata et al. 1999), Cysteine Rich
401 Protein 1 (Crip1) (Gava et al. 2008), and Insulin Like Growth Factor Binding Protein 5 (Igfbp5) (H. Wang et
402 al. 2006; Gava et al. 2008) which we validated herein. Despite their function in ovulatory wound repair, the
403 OSE gene expression was not drastically altered between the different stages of the estrous cycle, perhaps
404 due the small relative proportion of OSE participating in ovulation and subsequent wound repair and their
405 relatively low representation in the dataset. Nevertheless, we found genes previously associated to wound
406 healing such as Galectin 1 (Lgals1) (Lin et al. 2015), which were significantly upregulated in estrus when
407 compared to proestrus and metestrus. Interestingly, the Lgals1 knockout mice have delayed cutaneous
408 wound healing compared to their wild type counterparts (Hsieh et al. 2002). Similarly, the expression of the
409 immediate-early genes Fos, Jun, Junb, and Egr1 was variable during the estrous cycle, following a common
410 pattern of strong downregulation at estrous compared to the other stages. A potential explanation may be
411 the role of this gene family in stromal ovulatory wound repair, which would be consistent with previous
412 reports showing that mice with fibroblast overexpressing Egr1 exhibit exuberant tissue repair (Wu et al.
413 2009), while Jun, Fos and Fosb are in turn induced at different time points during corneal epithelial wound
414 healing (Okada et al. 1996).

415 The other cell types such as endothelial, immune cells and oocytes were found in the dataset but given
416 their relatively low representation, at 10%, 5% and 0.05% of all cells respectively, were not included in the
417 analysis of cyclic states. Other methodologies that include specific enrichment of these cell types should
418 be used to study their role in cyclic ovarian function.

419 Finally, to take advantage of this rich dataset, we sought to identify secreted markers which vary in
420 abundance during the estrous cycle and could thus be used as biomarkers in assisted reproduction. We
421 identified and prioritized four secreted biomarkers which varied significantly during different transitions of
422 the estrous cycle, namely Inhba, Prss35, Nppc, and Tinagl1.

423 Activin A is a secreted protein homodimer translated from the Inhba transcript that is a crucial modulator of
424 diverse ovarian functions including steroidogenesis and extracellular matrix remodeling, whose expression
425 level depends highly on the stage of the estrous cycle (Chang and Leung 2018). RNAscope analysis
426 confirmed that the transcript was mostly expressed by mural granulosa cells of antral follicles while qPCR
427 quantification found it to be highest in proestrus and quickly and significantly downregulated in estrous. In
428 contrast we found that the Activin A protein remained elevated in the blood in both proestrus and estrus,
429 which is consistent with studies in other species such as ewes . We speculate that
430 this pattern may reflect a delay between transcription and translation, a buildup of the Activin A protein in
431 the circulation, and the incorporation of the Inhba product into other dimers such as Inhibin A (Gedeon and
432 Bokes 2012).

433 The serine protease 35 transcript was expressed in the theca layers of preantral follicles and induced in
434 granulosa cells of preovulatory follicles and all stages of the corpora lutea, peaking at the estrous stage
435 according to qPCR, leading us to speculate that it may be involved tissue remodeling during ovulation and
436 corpus luteum formation (Wahlberg et al. 2008). In contrast, the PRSS35 protein levels were highest in the
437 diestrus and proestrus stages as determined by ELISA, suggesting perhaps there may be other extra-
438 ovarian sources of PRSS35 that are also cyclic.

439 The natriuretic peptide precursor C (NPPC) protein is a peptide hormone encoded by the Npcc gene. Nppc
440 has been reported to be expressed by mural granulosa cells while its receptor Npr2 is expressed by
441 cumulus cells. The pair acts on developing follicles by increasing the production of intracellular cyclic
442 guanosine monophosphate and maintains oocyte meiotic arrest while it matures; upon downregulation, the
443 oocyte can escape meiotic arrest and ovulate (Celik et al. 2019). This mechanism makes Nppc an
444 interesting marker to predict ovulation. Herein, qPCR analysis revealed that Nppc was highest in the ovary

445 at proestrus, and was quickly and significantly downregulated at estrous, probably in response to the
446 increased levels of LH which inhibits the Nppc/Npr2 system (Celik et al. 2015). In contrast there was a trend
447 for the circulating NPCC peptide to be highest in metestrus and diestrus, albeit not in a statistically
448 significant way.

449 Finally, we evaluated the level of transcription and protein expression of the matricellular factor Tinagl1. We
450 found both the Tinagl1 transcript and the circulating TINAGL1 protein in the blood to be highest during
451 estrous, thus coinciding with ovulation, with a pattern of expression consistent with mural granulosa cells
452 of antral follicles. While its role in the ovary has not been extensively investigated, it was associated with a
453 delayed decrease in the number of ovulated oocytes in aging Tinagl1 knock out mice due to delayed ovarian
454 collagen deposition (Akaiwa, Fukui, and Matsumoto 2020), Tinagl1 is known to be expressed in the uterus
455 in the decidual endometrium post implantation, and the Tinagl1 knockout mouse displays impaired fertility
456 characterized by the incapacity to carry pregnancy to term and perinatal lethality (Takahashi et al. 2016).
457 Recently, Tinagl1 was also shown to be involved in myofibroblast-mediated wound healing (Bergmeier et
458 al. 2018).

459 These potential cyclic biomarkers provide a proof of concept that a deeper understanding of changes at the
460 single cell transcriptomics may have useful applications in assisted reproduction. It will be of interest to
461 follow up the findings of cyclic expression of ACTIVIN A, PRSS35, NPPC, and TINAGL1, particularly in
462 combination as an index, for use in humans and other species for the purpose of assisted reproduction.

463 In summary, this study outlines dynamic mRNA expression in murine ovaries across the estrous cycle and
464 other reproductive states and extends our understanding of the diversity of cell types in the adult ovary. We
465 identified herein novel biomarkers of the estrous cycle that can be readily measured in the blood and may
466 have utility, in combination, to predict staging for assisted reproduction. This rich dataset will provide a
467 hypothesis-generating framework of cell states across the cycle with which to elucidate the complex cellular
468 interactions that are required for ovarian homeostasis.

469 Legends

470 **Figure 1 -** Single cell RNA sequencing of mouse cycling ovaries. A. Schematic of the pipeline applied to

471 single cell sequencing experiment. B. T-SNE plot featuring the different cell clusters of the ovary. C.
472 Heatmap presenting the top 10 markers of each cluster.

473 **Figure 2 -** Identification of the different cell types in the mesenchyme cluster A. T-SNE plot featuring the
474 different cell subclusters belonging to the mesenchyme cluster. B. Heatmap presenting the top 5 markers
475 of each cluster. C. Confirmation of each mesenchyme cluster with t-SNE-plots and RNA in situ hybridization

476 **Figure 3 -** Identification of the different cell types in granulosa cluster A. T-SNE plot featuring the different
477 cell subclusters belonging to the granulosa cluster. B. Heatmap presenting the top 5 markers of each
478 cluster. C. Confirmation of each granulosa cell cluster with RNA in situ hybridization

479 **Figure 4 -** Constructing single cell resolution trajectory of mesenchyme (A-C) and granulosa
480 clusters (D-F). A-C) Pseudo-temporal trajectory colored by cell types (A) and the splitting of each
481 group on the trajectory (B) of mesenchyme cluster, illustrated by a diagram of their developmental
482 progression (C). D-F) Pseudo-temporal trajectory colored by cell types (D) and the splitting of
483 each group on the trajectory (E) of granulosa cluster, illustrated by a diagram of their
484 developmental progression (F).

485 **Figure 5 -** Figure 4: Granulosa cell expressed genes vary in an estrous cycle dependent manner A. T-SNE
486 plot featuring the different estrous cycle stages in granulosa cell cluster. B. Volcano plot showing the genes
487 differentially expressed between proestrus and estrous stages. C. Left - Pathway analysis reveals enriched
488 pathways of differentially expressed genes (DEG) between the different stages of the estrous cycle. The x-
489
490 dot size, represents the number of genes enriched in a GO term and dot color represents the adjusted p
491 values. Right Gene networks of selected pathways are shown. Node size represents the number of genes
492
493 or downregulated. GO, Gene ontology; BP, Biological Process. D. QPCR validation of matrix remodeling
494 and steroidogenesis related markers (n=5 per group, mean ± SEM, *P<0.05, **P<0.01, ***P<0.005,
495 ****P<0.001).

496 **Figure 6 -** Figure 5: New secreted markers estrous cycle dependent. A. qPCR showing significant up and
497 downregulation of ovarian secreted markers depending on the stage of the estrous cycle (n=5 per group,
498 mean ± SEM, *P<0.05, **P<0.01, ***P<0.005). B. Expression levels and percentages of ovary secreted
499 markers in granulosa cells based on the different stages of the estrous cycle. C. In situ hybridization
500 (RNAscope) of the same markers. D. Quantification of blood circulating proteins by ELISA (n=5 per group,
501 mean ± SEM, *P<0.05, ***P<0.005). E. Summary of the ELISA results.

502 **Figure S2 -** Co-localization of smooth muscle marker Acta2 with Hhip and Mfap5
503 Feature plots (A.) showing colocalization of Acta2 and Hhip in the smooth muscle cluster and
504 expression of Mfap5 localized in the cluster theca 2, both confirmed by in situ hybridization/
505 IHC (B.)

506 **Figure S4 -** Heatmap representing the transcriptomic progression of dynamic genes in the cell
507 lineages of mesenchyme (A) and granulosa (B) clusters through the pseudotime. Early cells
508 common to both lineages are located in the center (Prebranch) of the map, with divergence to
509 two different cell fates to the sides.

510 **Figure S5 -** Estrus to Proestrus transition shows more genes dysregulated that any other stages A. Volcano
511 plot showing the genes differentially expressed between estrous and metestrous stages. B. Volcano plot
512 showing the genes differentially expressed between metestrous and diestrous stages. C. Volcano plot
513 showing the genes differentially expressed between diestrous and proestrous stages. D. T-SNE plot
514 featuring the ovarian surface epithelium (OSE) cells depending on the stage of the estrous cycle. E. QPCR
515 validation of ovarian surface epithelium expressed markers (n=5 per group, mean ± SEM, *P<0.05,
516 **P<0.01, ****P<0.001).

517 Acknowledgements
518 We thank LiHua Zhang, Caroline Coletti, and Sarah Mustafa Eisa for technical help. This study was
519 supported by the National Institute for Child Health and Human Development to D.P. (1R01HD102014-01),
520 the Huiying Fellowship (H.D.S.), Sudna Gar Fellowship (D.P.), Massachusetts General Hospital Executive

Committee on Research (D.P. and P.K.D.), and royalties (P.K.D.) from the use of the MIS ELISA in infertility clinics.

Bibliography

a a -like 1 Deficiency Alleviates Age-Dependent Depressed Ovulation Associated with Ovarian Collagen 5 *Reproductive Medicine and Biology* 19 (1): 50 57. https://doi.org/10.1002/rmb2.12301.

Bergmeier, Vera, Julia Etich, Lena Pitzler, Christian Frie, Manuel Koch, Matthias Fischer, Gunter Rappl, . . - *Society for Matrix Biology* 65 (January): 59 74. https://doi.org/10.1016/j.matbio.2017.07.005.

. a 5 *PloS One* 7 (4): e35538. https://doi.org/10.1371/journal.pone.0035538.

Celik, On D a t *Biochemistry Insights* 8: 11 21. https://doi.org/10.4137/BCI.S28596.

Celik, Onder, Nilufer Celik, Kader Ugur, Safak Hatirnaz, Sudenaz Celik, Iptisam Ipek Muderris, Seyda a a *Cellular and Molecular Biology (Noisy-Le-Grand, France)* 65 (4): 83 89.

Chang, Hsun-a t t *Journal of Bio-X Research* 1 (3). https://journals.lww.com/jbioxresearch/Fulltext/2018/12000/Physiological_roles_of_activins_in_the_human_ovary.2.aspx.

D 5 Expression in Granulosa Cells of Ovine Antral Growing Follicles Using Suppressive Subtractive Hybridiz *Animal Reproduction Science* 115 (1 4): 39 48. https://doi.org/10.1016/j.anireprosci.2008.10.022.

Deb, S., B. K. Campbell, J. S. Clewes, C. Pincott-Allen, and N. J. Raine- in Number of Antral Follicles Stratified by Size and in Endocrine Markers of Ovarian Reserve in a *Official Journal of the International Society of Ultrasound in Obstetrics and Gynecology* 41 (2): 216 22. https://doi.org/10.1002/uog.11226.

5 t *Biology of* a *Reproduction* 78 (1): 176 83. https://doi.org/10.1095/biolreprod.107.063537.

Fan, X., M. Bialecka, I. Moustakas, E. Lam, V. Torrens-Juaneda, N. V. Borggreven, L. Trouw, et al. 2019. - *Nature Communications* 10 (1): 3164. https://doi.org/10.1038/s41467-019-11036-9.

Gallardo, Teresa D., George B. John, Lane Shirley, Cristina M. Contreras, Esra A. Akbay, J. Marshall a 5 Discovery *Genetics* 177 (1): 179 94. https://doi.org/10.1534/genetics.107.074823.

Garside, Samantha A., Christopher R. Harlow, Stephen G. Hillier, Hamish M. Fraser, and Fiona H. rombospondin-1 Inhibits Angiogenesis and Promotes Follicular Atresia in a *Endocrinology* 151 (3): 1280 89. https://doi.org/10.1210/en.2009-0686.

Gava, Natalie, Christine L Clarke, Chris Bye, Karen Byth, and Anna deFazio. D D t *Journal of Molecular Endocrinology* 40 (6): 281 96. https://doi.org/10.1677/JME-07-0149.

D t . 5 ation between a t *Biophysical Journal* 103 (3): 377 85. https://doi.org/10.1016/j.bpj.2012.06.025.

Grosdemouge, Isabelle, Anne Bachelot, Aurélie Lucas, Nathalie Baran, Paul A. Kelly, and Nadine Binart. 5 t *Reproductive* 1 (February): 12. https://doi.org/10.1186/1477-7827-1-12.

Hartanti, M. D., K. Hummitzsch, H. F. Irving-Rodgers, W. M. Bonner, K. J. Copping, R. A. Anderson, I. C. a a t a of Stromal Expansion dur 5 *Reproduction, Fertility, and Development* 31 (3): 482 95. https://doi.org/10.1071/RD18218.

Hatzirodos, Nicholas, Helen F. Irving-Rodgers, Katja Hummitzsch, and Raymond J. Rodgers. 2014. t . *PloS One* 9 (6): e99706. https://doi.org/10.1371/journal.pone.0099706.

a a a D Expression of Wnts and Frizzleds at Specific Stages of Follicular Development in the Rodent *Endocrinology* 143 (3): 898 908. https://doi.org/10.1210/endo.143.3.8684.

Hummitzsch, Katja, Nicholas Hatzirodos, Anne M. Macpherson, Jeff Schwartz, Raymond J. Rodgers, and Helen F. Irving- *Reproduction (Cambridge, England)* 157 (6): 545 65. https://doi.org/10.1530/REP-18-0323.

. ingle-Cell RNA Sequencing Technologies and . *Experimental & Molecular Medicine* 50 (8): 1 14. https://doi.org/10.1038/s12276-018-0071-8.

Irving- a ulosa Cell Maturation in Dominant and Subordinate Bovine Follicles: Novel Extracellular Matrix Focimatrix Is Co-Ordinately Regulated with Cholesterol Side- *Reproduction (Cambridge, England)* 137 (5): 825 34. https://doi.org/10.1530/REP-08-0485.

Irving-Rodgers, Helen F., Katja Hummitzsch, Lydia S. Murdiyarso, Wendy M. Bonner, Yoshikazu Sado, Yoshifumi Ninomiya, John R. Couchman, Lydia M. Sorokin, and Raymond J. Rodgers. 2010. 5 a *Cell and Tissue Research* 339 (3): 613 24. https://doi.org/10.1007/s00441-009-0905-8.

a and Metallothionein Gene Expression in the Proliferating Epidermis during Wound Healing in a *Histochemistry and Cell Biology* 112 (4): 283 90. https://doi.org/10.1007/s004180050449.

Jevitt, Allison, Deeptiman Chatterjee, Gengqiang Xie, Xian-Feng Wang, Taylor Otwell, Yi-Chun Huang, and Wu-a 5 -Cell Atlas of Adult Drosophila Ovary Identifies Transcriptional t *PLoS Biology* 18 (4): e3000538. https://doi.org/10.1371/journal.pbio.3000538.

Kano, Motohiro, Amanda E. Sosulski, LiHua Zhang, Hatice D. Saatcioglu, Dan Wang, Nicholas Nagykery, a D D t 5

t *Proceedings of the National Academy of Sciences of the United States of America* 114 (9): E1688 97. https://doi.org/10.1073/pnas.1620729114.

Kenngott, Rebecca Anna-Maria, Ulrich Sauer, Margarete Vermehren, and Fred Sinowatz. 2014. arkers in the Developing Bovine Ovary: D An Immunohistochemical and Laser- a *Cells, Tissues, Organs* 200 (2): 153 70. https://doi.org/10.1159/000369203.

Kinnear, Hadrian M., Claire E. Tomaszewski, Faith L. Chang, Molly B. Moravek, Min Xu, Vasantha t *Reproduction (Cambridge, England)* 160 (3): R25 39. https://doi.org/10.1530/REP-19-0501.

Klein, Allon M., Linas Mazutis, Ilke Akartuna, Naren Tallapragada, Adrian Veres, Victor Li, Leonid Peshkin, 5 a -Cell Transcriptomics 5 *Cell* 161 (5): 1187 1201. https://doi.org/10.1016/j.cell.2015.04.044.

Lazzaro, Maribeth A., David Pépin, Nazario Pescador, Bruce D. Murphy, Barbara C. Vanderhyden, and 5 t t Regulatory Protein Expression during Terminal Differentiation of Ovarian Granulosa C *Molecular Endocrinology (Baltimore, Md.)* 20 (10): 2406 17. https://doi.org/10.1210/me.2005-0213.

Lin, Yueh-Te, Jhih-Sian Chen, Ming-Heng Wu, I.-Shan Hsieh, Chen-Hsien Liang, Cheng-Lung Hsu, Tse-Ming Hong, and Yuh- -1 Accelerates D Wound Healing by Regulating the Neuropilin- t t *The Journal of* a *Investigative Dermatology* 135 (1): 258 68. https://doi.org/10.1038/jid.2014.288.

Lussier, Jacques G., Mame N. Diouf, Valérie Lévesque Expression Profiling of Upregulated MRNAs in Granulosa Cells of Bovine Ovulatory Follicles D 15 (1): 88. https://doi.org/10.1186/s12958-017-0306-x.

Man, Limor, Nicole Lustgarten-Guahmich, Eleni Kallinos, Zachary Redhead-Laconte, Sally Liu, Benjamin 5 versus Ovarian Origin Reveals Disparate Molecular *Cell Reports* 32 (6): 108027. https://doi.org/10.1016/j.celrep.2020.108027.

Meinsohn, Marie-Charlotte, Hatice D. Saatcioglu, Lina Wei, Yi Li, Heiko Horn, Maeva Chauvin, Motohiro -Cell Sequencing Reveals Suppressive Transcriptional Programs a a *Proceedings of the National Academy of Sciences of the United States of America* 118 (20). https://doi.org/10.1073/pnas.2100920118.

Melo, E. O., D. M. Cordeiro, R. Pellegrino, Z. Wei, Z. J. Daye, R. C. Nishimura, and M. A. N. Dode. 2017. a a *Animal Genetics* 48 (1): 19 29. https://doi.org/10.1111/age.12496.

Nakagawa, Shinichi, Masayuki Shimada, Kaori Yanaka, Mari Mito, Takashi Arai, Eiki Takahashi, Youko t *Development (Cambridge, England)* a 141 (23): 4618 27. https://doi.org/10.1242/dev.110544.

5 *Proceedings of the National Academy of Sciences of the United States of America* 117 (33): 20015 26. https://doi.org/10.1073/pnas.2005570117.

t a t Reader, Peter D. Johnstone, George H. Davis,

The Journal of Endocrinology t
228 (3): 193 203. https://doi.org/10.1530/JOE-15-0367.
Okada, Y., S. Saika, N. Hashizume, S. Kobata, O. Yamanaka
Fos Family and Jun Family Proto- *Current*
Eye Research 15 (8): 824 32. https://doi.org/10.3109/02713689609017623.
Pépin, D., M. Hoang, F. Nicolaou, K. Hendren, L. A. Benedict, A. Al-Moujahed, A. Sosulski, A. Marmalidou,
5 t 5
Modification Enhances the Yield of Recombinant C- a
Technology (Elmsford, N.Y.) 1 (1): 63 71. https://doi.org/10.1142/S2339547813500076.
Piersanti, Rachel L., José E. P. Santos, I. Martin Sheldon, and John J. Bromfield. 2019.
-Alpha Alter Gene Expression of Oocytes and
Cu . *Molecular Reproduction and Development* 86
(12): 1909 20. https://doi.org/10.1002/mrd.23288.
a
Hormones o *Physiological Reviews* 60 (1): 51 89.
https://doi.org/10.1152/physrev.1980.60.1.51.
Richards, JoAnne S., Yi A. Ren, Nicholes Candelaria, Jaye E. Adams, and Aleksandar Rajkovic. 2018.
ment, Differentiation, and Impact on Fertility: 2017
Endocrine Reviews 39 (1): 1 20. https://doi.org/10.1210/er.2017-00164.
t .
The Journal of Clinical Endocrinology & Metabolism 26 (1): 46 52. https://doi.org/10.1210/jcem-
26-1-46.
Saatcioglu, Hatice Duygu, Motohiro Kano, Heiko Horn, Lihua Zhang, Wesley Samore, Nicholas Nagykery,
Marie- a -Cell Sequencing of Neonatal Uterus Reveals an
a t *ELife* 8 (June).
https://doi.org/10.7554/eLife.46349.
Sayasith, Khampoun, Jacques Lussier, and Jean Sirois. a
Transcriptional Regulation of a Disintegrin and Metalloproteinase with Thrombospondin Motif 1
5 a . t *Endocrinology* 154 (8): 2857 69.
https://doi.org/10.1210/en.2013-1140.
Stévant, Isabelle, Françoise Kühne, Andy Greenfield, Marie-Christine Chaboissier, Emmanouil T.
5 5
Determination in Gonadal Somatic Cells Using Single- *Cell Reports* 26 (12):
3272-3283.e3. https://doi.org/10.1016/j.celrep.2019.02.069.
Takahashi, Akihito, Ajalli Rahim, Miki Takeuchi, Emiko Fukui, Midori Yoshizawa, Kuniaki Mukai, Makoto
a
Female Fertility in Tubulointerstitial Antigen-like 1-Deficient Mic *The Journal of Reproduction*
and Development 62 (1): 43 49. https://doi.org/10.1262/jrd.2015-109.
Terenina, Elena, Stephane Fabre, Agnès Bonnet, Danielle Monniaux, Christèle Robert-Granié, Magali
SanCristobal, Julien Sarry, et al. 2017. 5 Expressed Genes and Gene Networks
t *Physiological Genomics* 49 (2): 67 80.
https://doi.org/10.1152/physiolgenomics.00069.2016.
pondin-1
Endocrinology 149 (1):
185 92. https://doi.org/10.1210/en.2007-0835.
Trapnell, Cole, Davide Cacchiarelli, Jonna Grimsby, Prapti Pokharel, Shuqiang Li, Michael Morse, Niall J.
a

5 t
Nature Biotechnology 32 (4): 381 86. https://doi.org/10.1038/nbt.2859.
Wagner, Magdalena, Masahito Yoshihara, Iyadh Douagi, Anastasios Damdimopoulos, Sarita Panula, Sophie Petropoulos, Haojiang Lu, et al. 2020. -Cell Analysis of Human Ovarian Cortex 5 t *Nature Communications* 11 (1): 1147. https://doi.org/10.1038/s41467-020-14936-3.
t
the Serine Proteases High-Temperature Requirement Factor A1, Serine Protease 23, and Serine t *Endocrinology* 149 (10): 5070 77. https://doi.org/10.1210/en.2007-1736.
Wang, Huamin, Daniel G. Rosen, Hua Wang, Gregory N. Fuller, Wei Zhang, and Jinsong Liu. 2006. -like Growth Factor-Binding Protein 2 and 5 Are Differentially Regulated in Ovarian 5 *States and Canadian Academy of Pathology, Inc* 19 (9): 1149 56. https://doi.org/10.1038/modpathol.3800637.
Wan t 5 D a a 5 *International Journal of Molecular Sciences* 19 (7). https://doi.org/10.3390/ijms19072028.
- *Cell* 180 (3): 585-600.e19. https://doi.org/10.1016/j.cell.2020.01.009.
Wigglesworth, Karen, Kyung-Bon Lee, Chihiro Emori, Koji Sugiura, and John J. Eppig. 2015. 5 5 *Biology of Reproduction* 92 (1): 23. https://doi.org/10.1095/biolreprod.114.121756.
Wu, Minghua, Denisa S. Melichian, Mauricio de la Garza, Katherine Gruner, Swati Bhattacharyya, Luke . - *The American Journal of Pathology* 175 (3): 1041 55. https://doi.org/10.2353/ajpath.2009.090241.
Xu, Fuhua, Richard L. Stouffer, Jörg Müller, Jon D. Hennebold, Jay W. Wright, Alistair Bahar, Gabriele 5 *Molecular Human Reproduction* 17 (3): 152 65. https://doi.org/10.1093/molehr/gaq089.
Zhao, Zheng-Hui, Jun-Yu Ma, Tie-Gang Meng, Zhen-Bo Wang, Wei Yue, Qian Zhou, Sen Li, et al. 2020. -Cell RNA Sequencing Reveals the Landscape of D 5 *Biology* 34 (9): 12634 45. https://doi.org/10.1096/fj.202001034RR.
Zhu, Weihua, Min Yang, Jinnan Shang, Yiliang Xu, Yuanlang Wang, Qiangqiang Tao, Liang Zhang, et al. -222 Inhibits Apoptosis in Porcine Follicular Granulosa Cells by Targeting the THBS1 D *Animal Science Journal = Nihon Chikusan Gakkaiho* 90 (6): 719 27. https://doi.org/10.1111/asj.13208.

Figure 1

A.

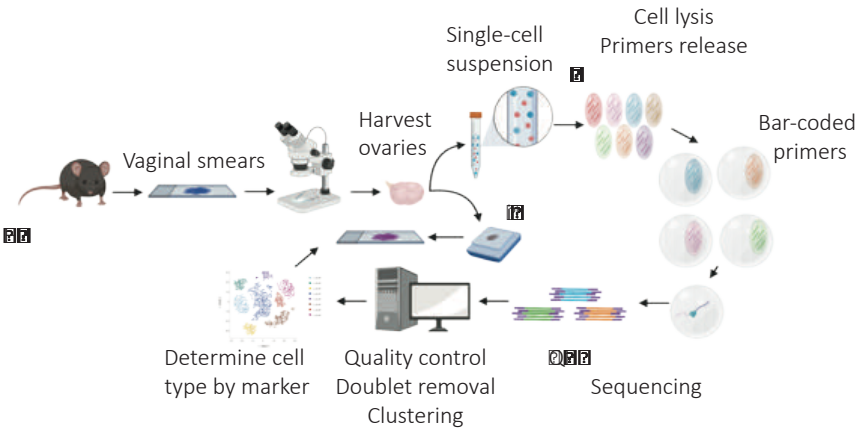
Vaginal smears
Harvest ovaries
Single-cell suspension
Cell lysis
Primers release
Bar-coded primers
Determine cell type by marker
Quality control
Doublet removal
Clustering
Sequencing

B.

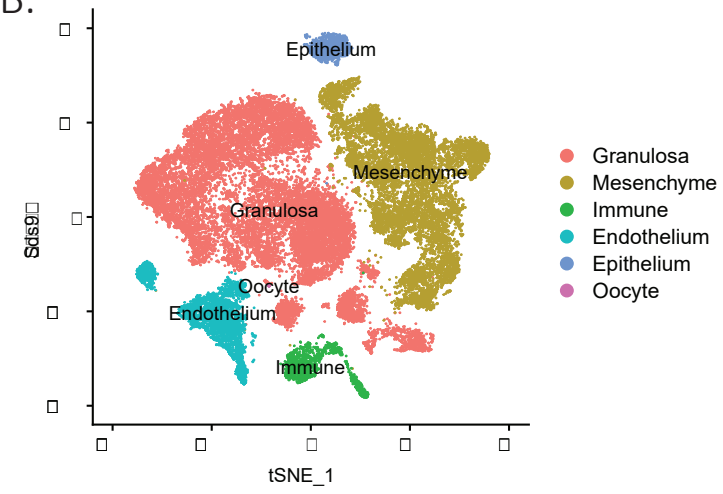
Epithelium
Mesenchyme
Granulosa
Oocyte
Endothelium
Immune
tSNE_1
Granulosa
Mesenchyme
Immune
Endothelium
Epithelium
Oocyte

C.

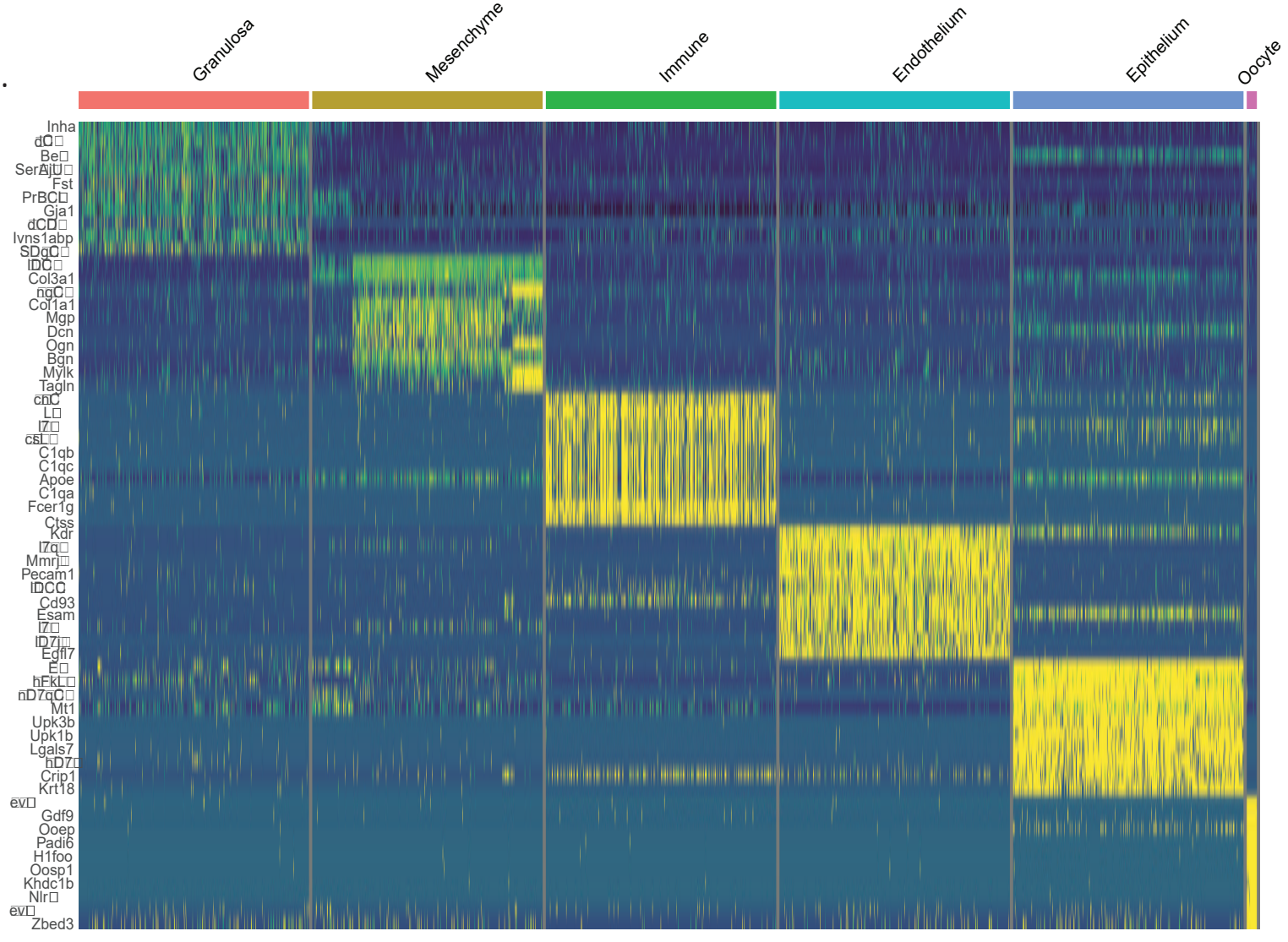
Granulosa
Mesenchyme
Immune
Endothelium
Epithelium
Oocyte
Inha
Fst
Gja1
Ivns1abp
Col3a1
Col1a1
Mgp
Dcn
Ogn
Bgn
Mylk
Tagln
C1qb
C1qc
Apoe
C1qa
Fcer1g
Ctss
Kdr
Pecam1
Cd93
Esam
Egfl7
Mt1
Upk3b
Upk1b
Lgals7
Crip1
Krt18
Gdf9
Ooep
Padi6
H1foo
Oosp1
Khdc1b
Zbed3

Figure 2

A.

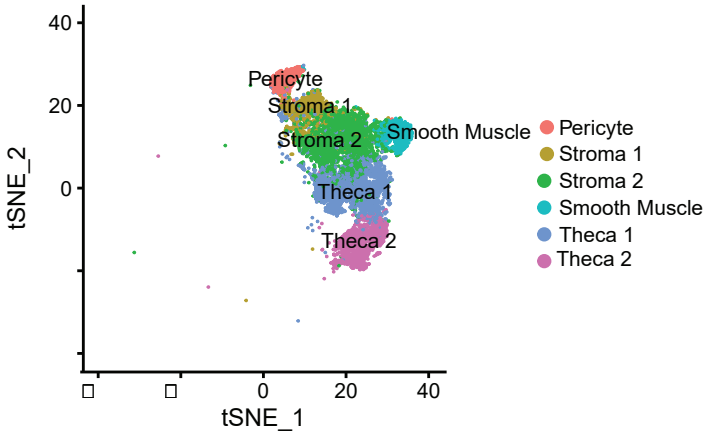

B.

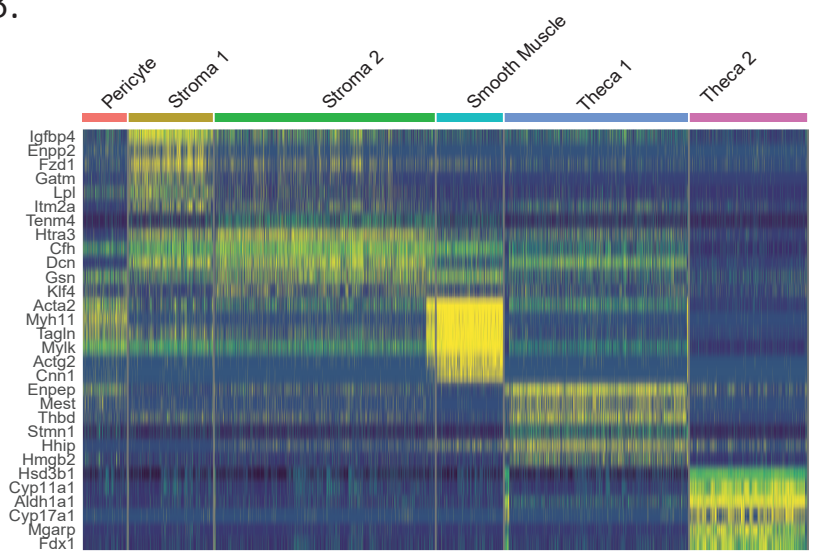

C.

Smooth muscle-***Mfap5***

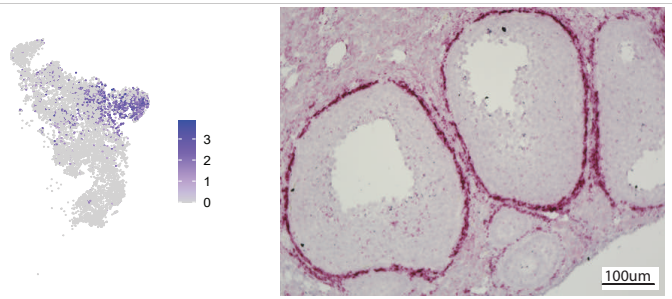

Stroma 1-***Enpp2***

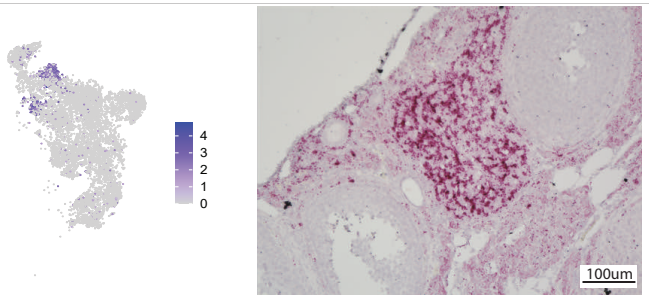

Stroma 2- ***Kcnk2***

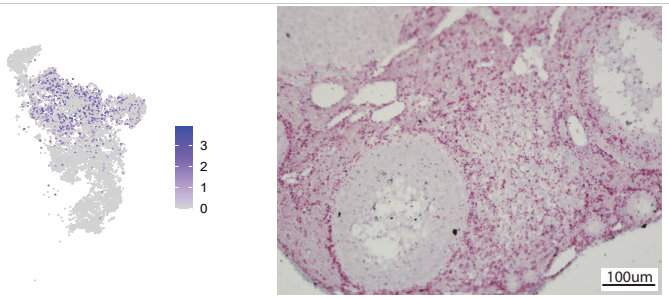

Theca 1- ***Cd24a***

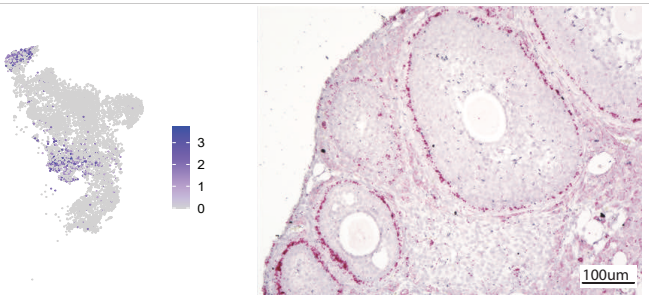

Theca 1- ***Hhip***

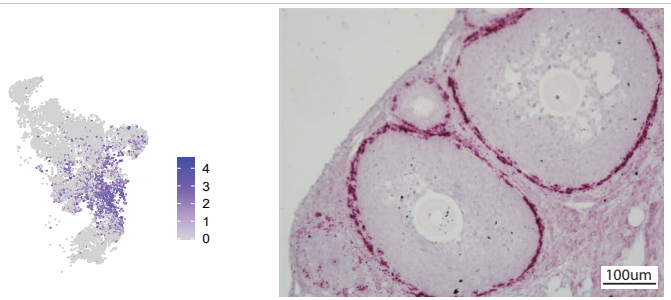

Theca 2- ***Cyp17a1***

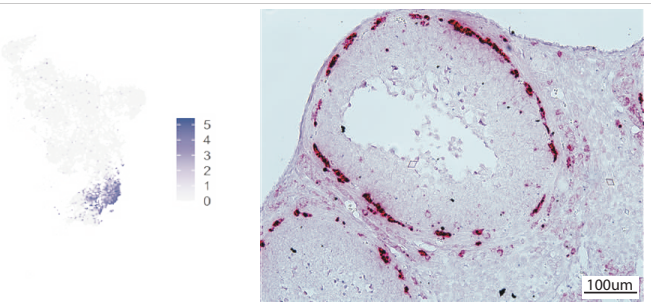

Figure 3

A.

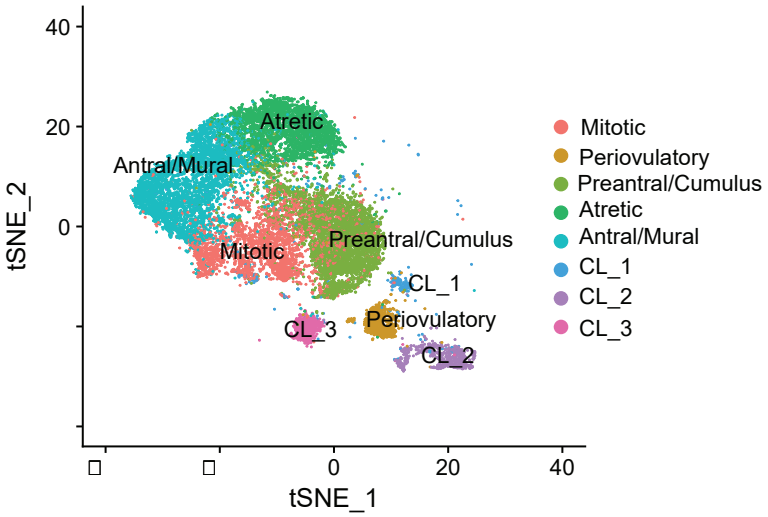

B.

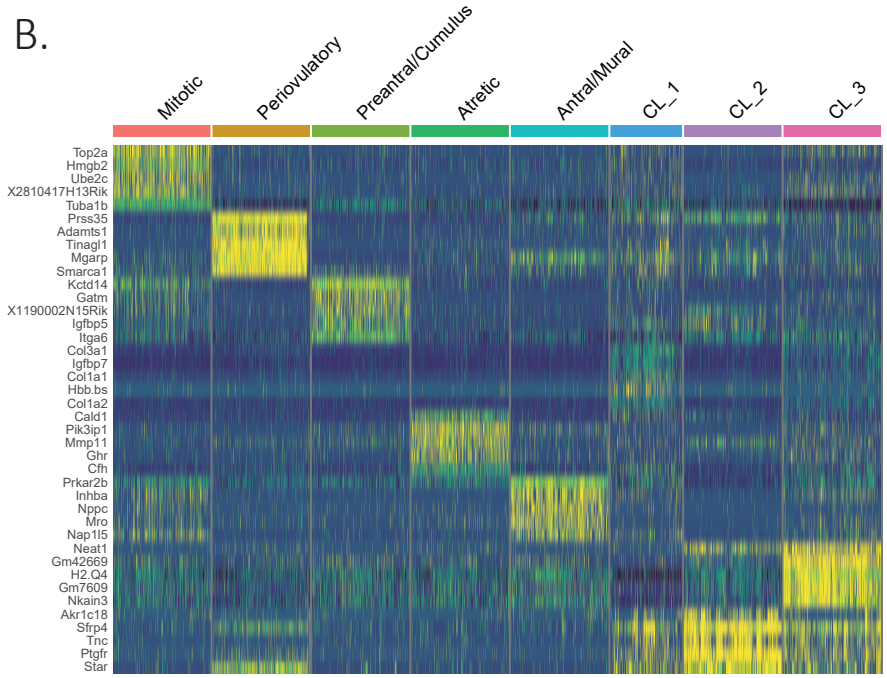

C.

*Atretic-**Ghr***

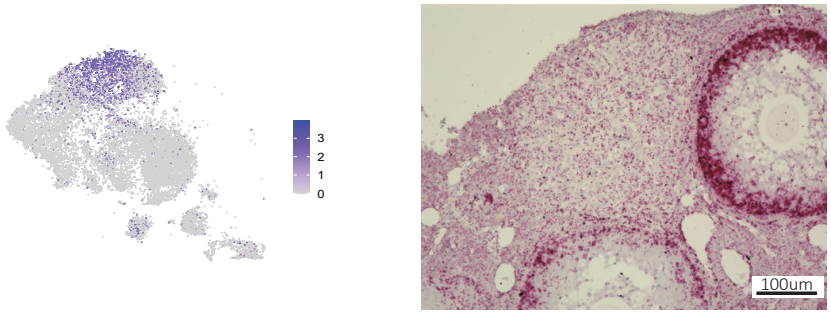

*Preantral Cumulus-**Kctd14***

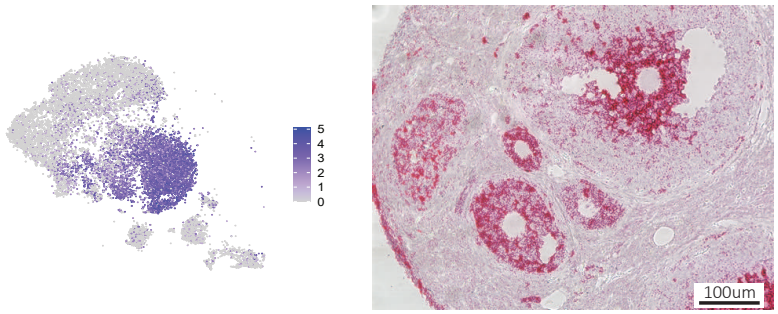

*Periovulatory-**Runx1***

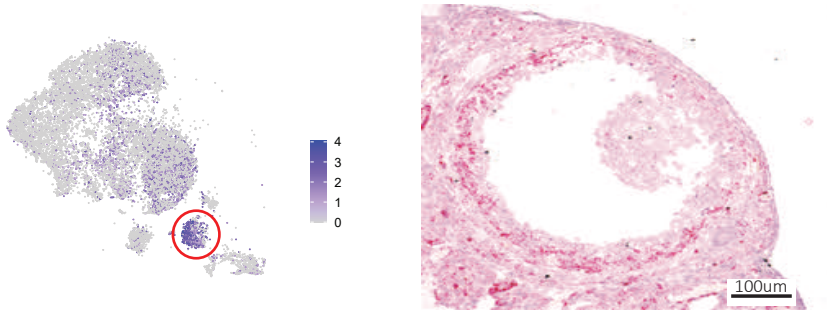

*CL-**Onecut 2***

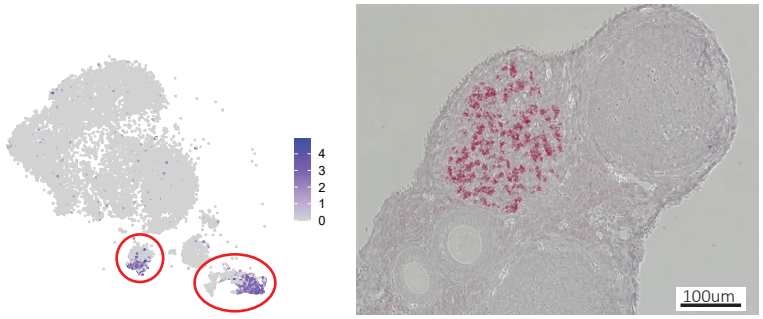

*Antral Mural-**Mro***

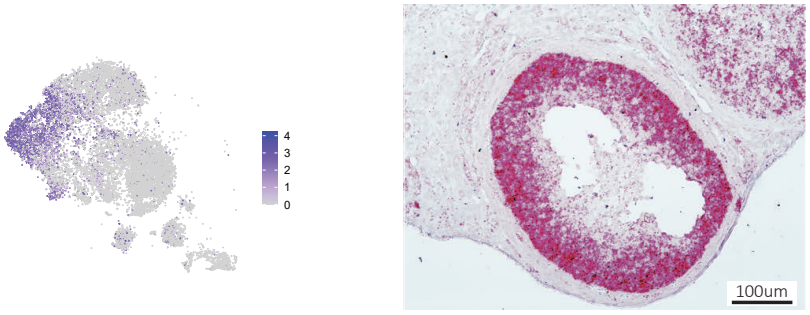

*Mitotic-**Top2a***

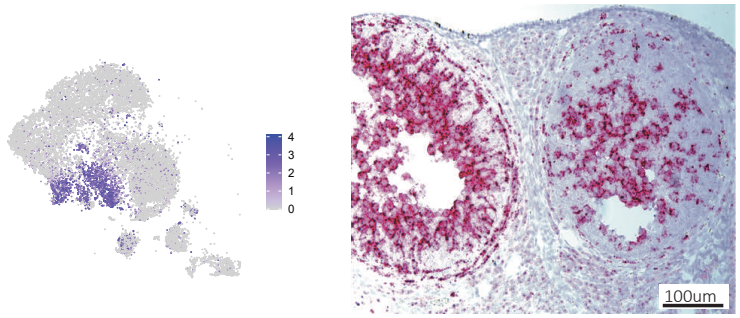

Figure 4

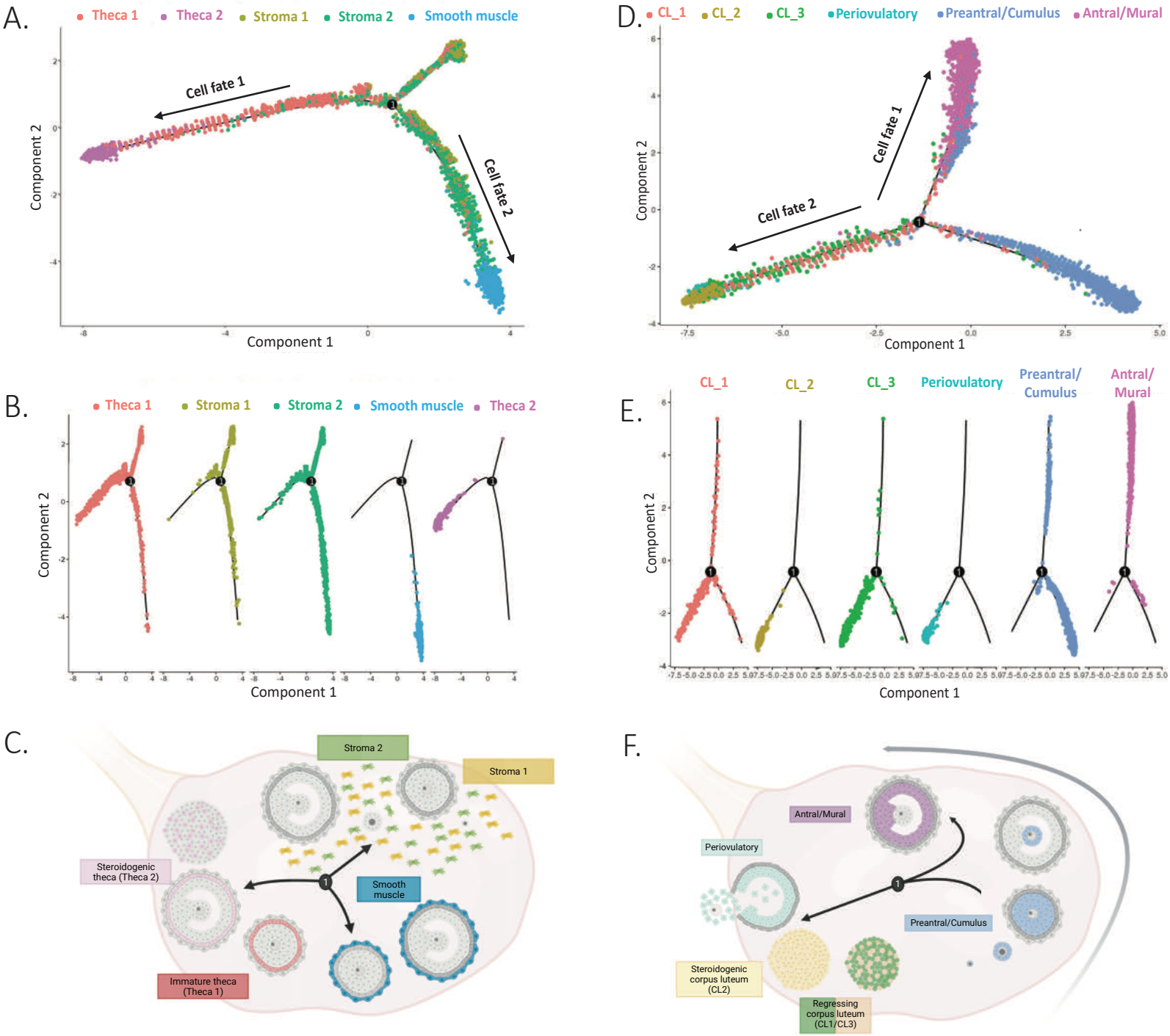
A.
Theca 1
Theca 2
Stroma 1
Stroma 2
Smooth muscle
Cell fate 1
Cell fate 2
Component 1
Component 2
D.
CL_1
CL_2
CL_3
Periovulatory
Preantral/Cumulus
Antral/Mural
Cell fate 1
Cell fate 2
Component 1
Component 2
B.
Theca 1
Stroma 1
Stroma 2
Smooth muscle
Theca 2
Component 1
Component 2
E.
CL_1
CL_2
CL_3
Periovulatory
Preantral/ Cumulus
Antral/ Mural
Component 1
Component 2
C.
Stroma 2
Stroma 1
Steroidogenic theca (Theca 2)
Smooth muscle
Immature theca (Theca 1)
F.
Antral/Mural
Periovulatory
Preantral/Cumulus
Steroidogenic corpus luteum (CL2)
Regressing corpus luteum (CL1/CL3)

Figure 5

A.

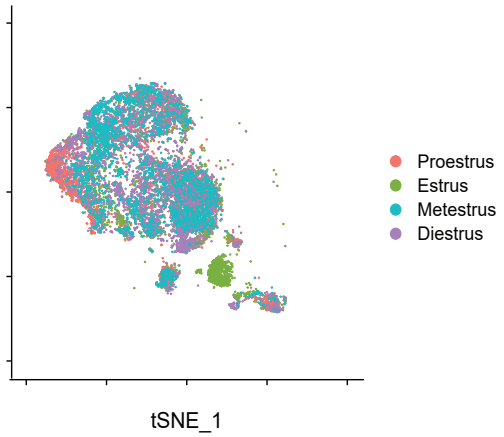

B.

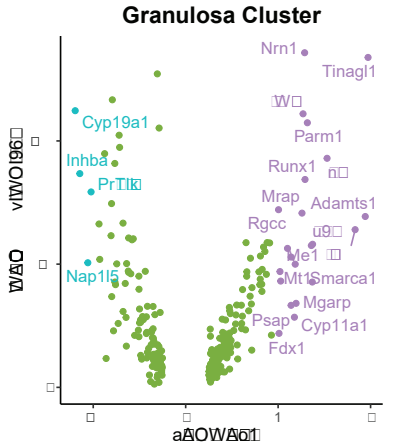

C.

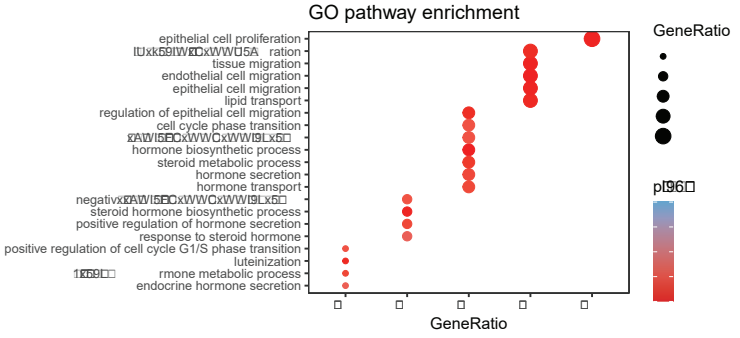

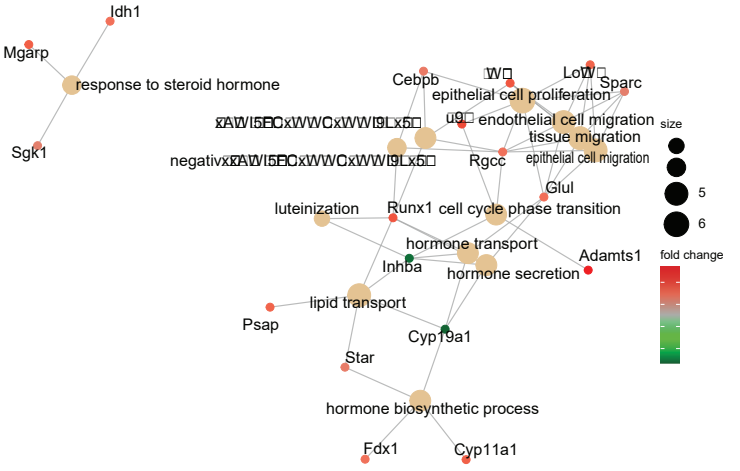

D.

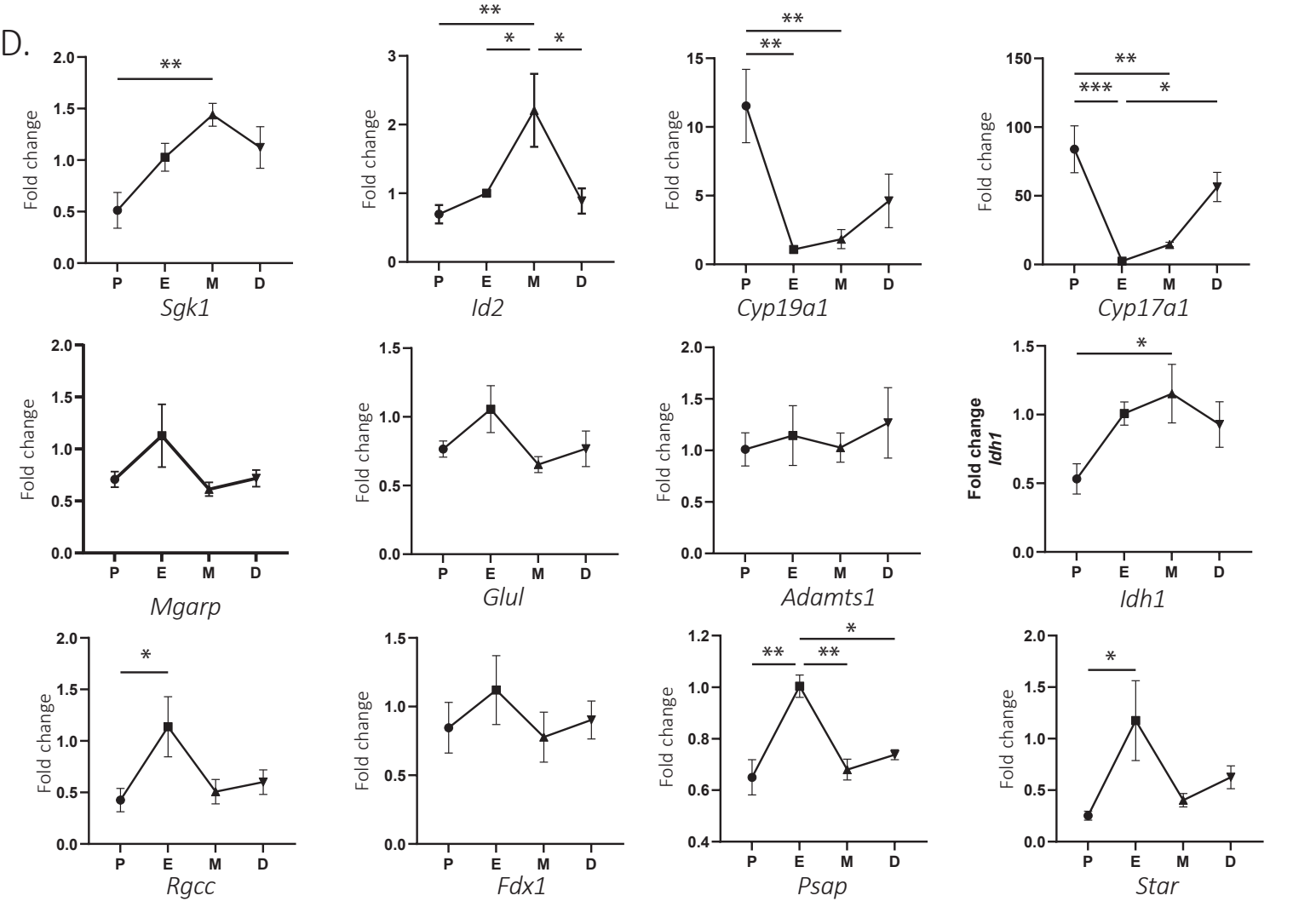

Figure 6

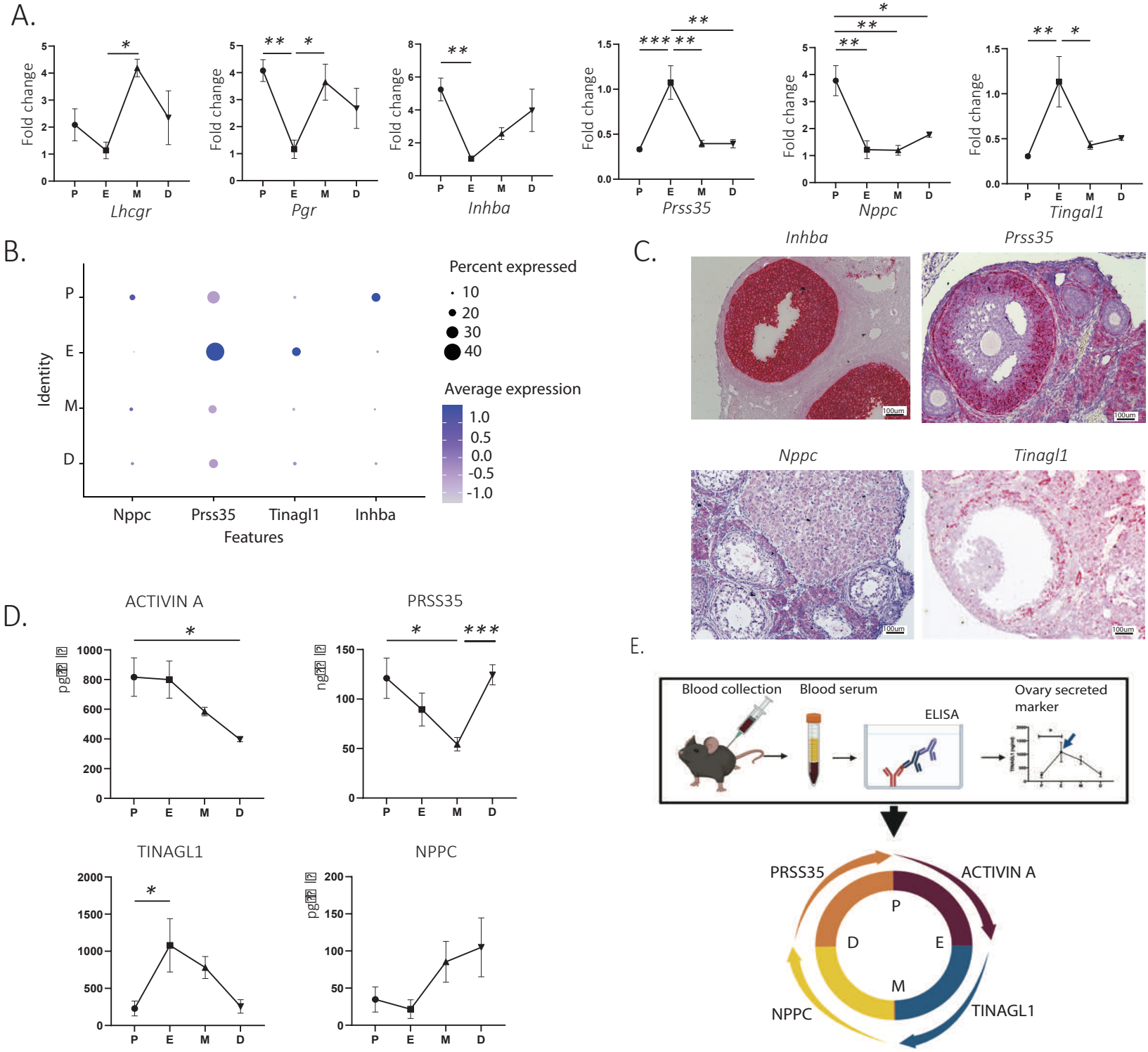
A.
Fold change
P
E
M
D
Lhcgr
Pgr
Inhba
Prss35
Nppc
Tingal1
B.
Identity
Features
Nppc
Prss35
Tinagl1
Inhba
Percent expressed
10
20
30
40
Average expression
1.0
0.5
0.0
-0.5
-1.0
C.
Inhba
Prss35
Nppc
Tinagl1
100um
D.
ACTIVIN A
PRSS35
TINAGL1
NPPC
pg/ml
ng/ml
E.
Blood collection
Blood serum
ELISA
Ovary secreted marker
PRSS35
ACTIVIN A
NPPC
TINAGL1
P
E
M
D

Figure S2

A.

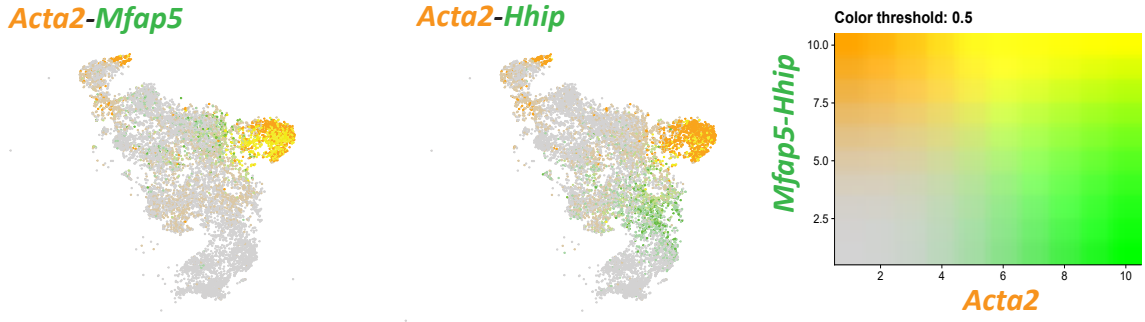
Acta2-Mfap5
Acta2-Hhip
Color threshold: 0.5
Mfap5-Hhip
10.0
7.5
5.0
2.5
2
4
6
8
10
Acta2

B.

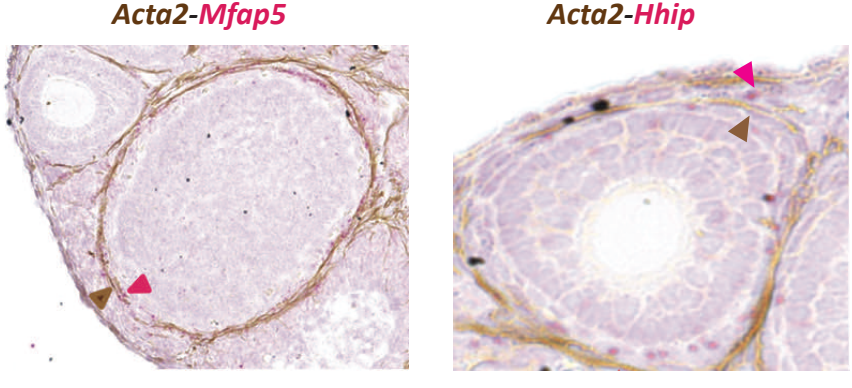
Acta2-Mfap5
Acta2-Hhip

Figure S4

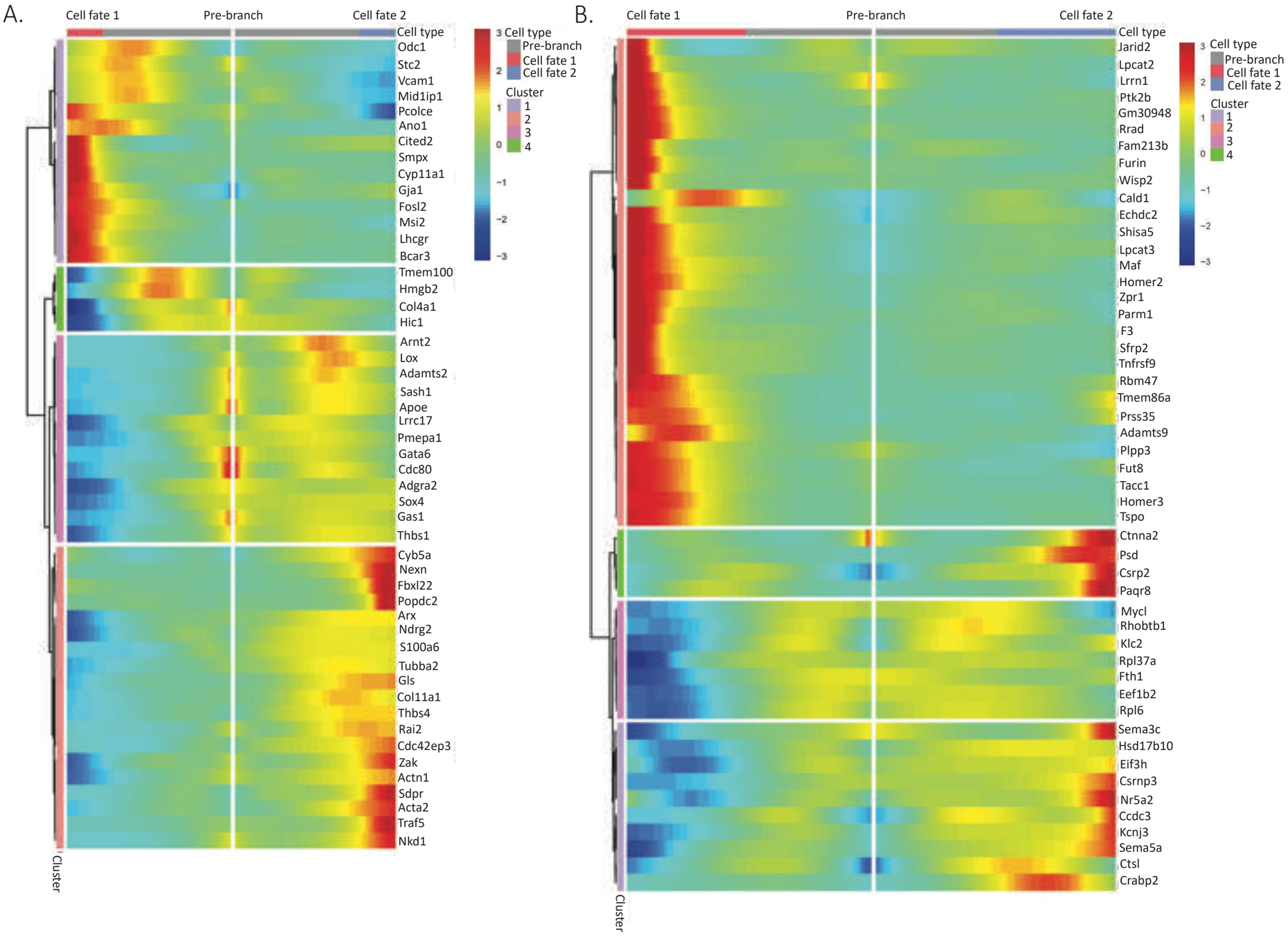
A.
Cell fate 1
Pre-branch
Cell fate 2
Cell type
Odc1
Stc2
Vcam1
Mid1ip1
Pcolce
Ano1
Cited2
Smpx
Cyp11a1
Gja1
Fosl2
Msi2
Lhcgr
Bcar3
Tmem100
Hmgb2
Col4a1
Hic1
Arnt2
Lox
Adamts2
Sash1
Apoe
Lrrc17
Pmepa1
Gata6
Cdc80
Adgra2
Sox4
Gas1
Thbs1
Cyb5a
Nexn
Fbxl22
Popdc2
Arx
Ndrg2
S100a6
Tubba2
Gls
Col11a1
Thbs4
Rai2
Cdc42ep3
Zak
Actn1
Sdpr
Acta2
Traf5
Nkd1
Cluster
3
2
1
0
−1
−2
−3
Cell type
Pre-branch
Cell fate 1
Cell fate 2
Cluster
1
2
3
4
B.
Cell fate 1
Pre-branch
Cell fate 2
Cell type
Jarid2
Lpcat2
Lrrn1
Ptk2b
Gm30948
Rrad
Fam213b
Furin
Wisp2
Cald1
Echdc2
Shisa5
Lpcat3
Maf
Homer2
Zpr1
Parm1
F3
Sfrp2
Tnfrsf9
Rbm47
Tmem86a
Prss35
Adamts9
Plpp3
Fut8
Tacc1
Homer3
Tspo
Ctnna2
Psd
Csrp2
Paqr8
Mycl
Rhobtb1
Klc2
Rpl37a
Fth1
Eef1b2
Rpl6
Sema3c
Hsd17b10
Eif3h
Csrnp3
Nr5a2
Ccdc3
Kcnj3
Sema5a
Ctsl
Crabp2
Cluster
3
2
1
0
−1
−2
−3
Cell type
Pre-branch
Cell fate 1
Cell fate 2
Cluster
1
2
3
4

Figure S5

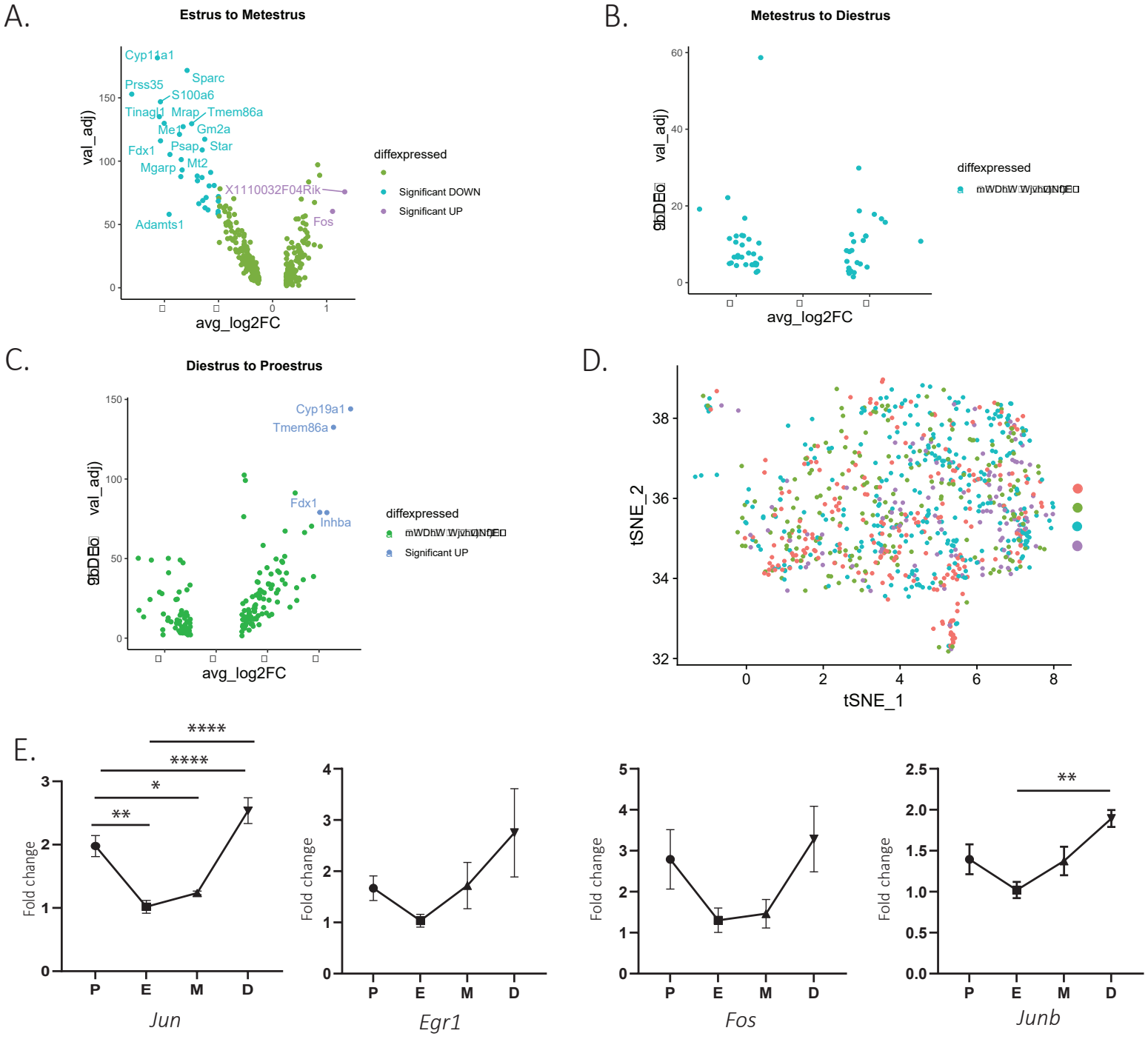
A.
Estrus to Metestrus
Cyp11a1
Sparc
Prss35
S100a6
Tinagl1
Mrap
Tmem86a
Me1
Gm2a
Fdx1
Psap
Star
Mgarp
Mt2
X1110032F04Rik
Adamts1
Fos
val_adj)
avg_log2FC
diffexpressed
Significant DOWN
Significant UP
B.
Metestrus to Diestrus
val_adj)
avg_log2FC
diffexpressed
C.
Diestrus to Proestrus
Cyp19a1
Tmem86a
Fdx1
Inhba
val_adj)
avg_log2FC
diffexpressed
Significant UP
D.
tSNE_2
tSNE_1
E.
Fold change
P
E
M
D
Jun
Egr1
Fos
Junb